A modeling study of ionospheric F2-region storm effects at low geomagnetic latitudes during 17-22 March 1990

A. V. Pavlov, S. Fukao, S. Kawamura

Ann. Geophys., 24, 915–940, 2006
www.ann-geophys.net/24/915/2006/

Annales Geophysicae

A modeling study of ionospheric F2-region storm effects at low geomagnetic latitudes during 17–22 March 1990

A. V. Pavlov[1], **S. Fukao**[2], **and S. Kawamura**[3]

[1]Pushkov Institute of Terrestrial Magnetism, Ionosphere and Radio-Wave Propagation, Russian Academy of Science (IZMIRAN), Troitsk, Moscow Region, 142190, Russia
[2]Research Institute for Sustainable Humanosphere (RISH), Kyoto University, Kyoto, 611-0011, Japan
[3]National Institute of Information and Communications Technology, 4-2-1, Nukui-kita, Koganei, Tokyo 184-8795, Japan

Received: 6 September 2005 – Revised: 9 March 2006 – Accepted: 23 March 2006 – Published: 19 May 2006

Abstract. We have presented a comparison between the modeled *Nm*F2 and *hm*F2, and *Nm*F2 and *hm*F2, which were observed in the low-latitude ionosphere simultaneously by the Kokubunji, Yamagawa, Okinawa, Manila, Vanimo, and Darwin ionospheric sounders, by the middle and upper atmosphere (MU) radar during 17–22 March 1990, and by the Arecibo radar for the time period of 20–22 March 1990. A comparison between the electron and ion temperatures measured by the MU and Arecibo radars and those produced by the model of the ionosphere and plasmasphere is presented. The empirical zonal electric field, the meridional neutral wind taken from the HWM90 wind model, and the NRLMSISE-00 neutral temperature and densities are corrected so that the model results agree reasonably with the ionospheric sounder observations, and the MU and Arecibo radar data. It is proved that the nighttime weakening of the equatorial zonal electric field (in comparison with that produced by the empirical model of Fejer and Scherliess (1997) or Scherliess and Fejer (1999)), in combination with the corrected wind-induced plasma drift along magnetic field lines, provides the development of the nighttime enhancements in *Nm*F2 observed over Manila during 17–22 March 1990. As a result, the new physical mechanism of the nighttime *Nm*F2 enhancement formation close to the geomagnetic equator includes the nighttime weakening of the equatorial zonal electric field and equatorward nighttime plasma drift along magnetic field lines caused by neutral wind in the both geomagnetic hemispheres. It is found that the latitudinal positions of the crests depend on the $\boldsymbol{E}\times\boldsymbol{B}$ drift velocity and on the neutral wind velocity. The relative role of the main mechanisms of the equatorial anomaly suppression observed during geomagnetic storms is studied for the first time in terms of storm-time variations of the model crest-to-trough ratios of the equatorial anomaly. During most of the studied time period, a total contribution from meridional neutral winds and variations in the zonal electric field to the equatorial anomaly changes is larger than that from geomagnetic storm disturbances in the neutral temperature and densities. Vibrationally excited N_2 and O_2 promote the equatorial anomaly enhancement during the predominant part of the studied time period, however, the role of vibrationally excited N_2 and O_2 in the development of the equatorial anomaly is not significant. The asymmetries in the neutral wind and densities relative to the geomagnetic equator are responsible for the north-south asymmetry in *Nm*F2 and *hm*F2, and for the asymmetry between the values of the crest-to-trough ratios of the Northern and Southern Hemispheres. The model simulations provide evidence in favor of an asymmetry in longitude of the energy input into the auroral region of the Northern Hemisphere on 21 March 1990.

Keywords. Ionosphere (Electric fields and currents; Equatorial ionosphere; Plasma temperature and density; Ionospheric disturbances; Modeling and forecasting)

1 Introduction

Geomagnetic storm effects on the ionosphere depend on season, latitude, and longitude, as well as on the severity, time of occurrence, and duration of the storm, and the geomagnetic storm changes in electric fields, thermospheric winds and neutral composition have been suggested to explain variations in the low-latitude ionosphere (Abdu et al., 1991; Abdu, 1997; Buonsanto, 1999; Rishbeth, 1975, 2000; Pavlov et al., 2004b and references therein). The storm-time F-region changes at low geomagnetic latitudes have been identified from F-layer height and frequency responses observed by ionosondes (see Abdu, 1997 and references therein). The dynamics of the low-latitude ionosphere was observed by the middle and upper atmosphere (MU) radar during the

Correspondence to: A. V. Pavlov
(pavlov@izmiran.rssi.ru)

Published by Copernicus GmbH on behalf of the European Geosciences Union.

geomagnetic storms of 6–8 February 1986, 20–21 January 1989, 20–23 October 1989, and 25–27 August 1987 (Oliver et al., 1988; Reddy et al., 1990; Oliver et al., 1991; Pavlov et al., 2004b). The changes in F-layer electron density observed by the MU radar in the 6–8 February 1986 storm were explained by changes in an influx of ionization from the plasmasphere, modulated by the passage of a large-scale, southward traveling gravity wave (Oliver et al., 1988). In the 20–21 January 1989 storm, the observed large changes in the F2-region peak altitude from 23:00 LT to 02:40 LT were attributed to a large eastward electric field originating at auroral latitudes (Reddy et al., 1990). During the 20–23 October 1989 storm-time period, drastically different electron densities were discovered in the F-region (Oliver et al., 1991). Pavlov et al. (2004b) have presented a comparison of the modeled F2-layer peak densities, *Nm*F2, and altitudes, *hm*F2, with *Nm*F2 and *hm*F2, which were observed at low geomagnetic latitudes simultaneously by the Akita, Kokubunji, Yamagawa, Okinawa, Manila, Vanimo, and Darwin ionospheric sounders and by the MU radar during the 25–27 August 1987 geomagnetically storm, taking into account the storm-time changes in the thermospheric wind, the electric field, the neutral composition, and the neutral temperature. It is found by Pavlov et al. (2004b) that the geomagnetic latitude variations in *Nm*F2, calculated for 26 August 1987 (the recovery phase of the geomagnetic storm), differ significantly from those calculated for 25 August 1987 (before SSC and during the main phase of the geomagnetic storm) and for 27 August 1987 (after the geomagnetic storm). The Arecibo radar observations of the ionospheric F-region during the 1–5 May 1995 geomagnetic storm period have shown that there is the possibility of poleward expansion of the equatorial anomaly zone with the northern anomaly crest location close to the 29° dip latitude (Buonsanto, 1999). Another anomalous low-latitude ionospheric feature was observed during the 17–18 February 1999 highly disturbed geomagnetic period, when the Arecibo radar recorded an anomalous nighttime ionospheric enhancement in which the nighttime value of *Nm*F2 exceeded 10^6 cm^{-3} and the F2 peak altitude went above 400 km (Aponte et al., 2000).

The effects of geomagnetic storms on the low-latitude ionosphere and plasmasphere have attracted much interest. The simplified theoretical computations of Burge et al. (1973) and Chandra and Spencer (1976) have speculated on the importance of the disturbed neutral winds to the low-latitude ionospheric response to geomagnetic storms, but lack of data and/or model winds has hampered progress. Ignoring electric field perturbations, due to the storm during 22 March 1979, and suggesting that the temperatures of electrons and ions are equal to the neutral temperature, Fesen et al. (1989) found that the equatorial anomaly may be disrupted by the magnetic storms, and that the major factor influencing the storm-time ionospheric behavior is the neutral wind. Variations in the low-latitude ionosphere for a hypothetical geomagnetic storm at equinox and high solar activity were studied by Fuller-Rowell et al. (2002), without taking into account geomagnetic storm disturbances in the electric field. Their model results made clear the difference between the effects of meridional and zonal winds on the disturbed ionosphere.

Electric fields $\boldsymbol{E}$ affect the distribution of plasma in the low-latitude ionospheric F-region, causing both ions and electrons to drift in the same direction with a drift velocity, $\boldsymbol{V}^E=\boldsymbol{E}\times\boldsymbol{B}/\mathrm{B}^2$, perpendicular to the geomagnetic field $\boldsymbol{B}$ direction. The present work studies the relationship between variations in the meridional component of $\boldsymbol{V}^E$ and the dynamics of the low-latitude F2-layer in the low-latitude ionosphere, when *Nm*F2 and *hm*F2 are observed simultaneously by the Kokubunji, Yamagawa, Okinawa, Manila, Vanimo, and Darwin ionospheric sounders and by the MU and Arecibo radars during the 17–22 March 1990 geomagnetically storm-time period. We investigate how well the measured electron density and temperature at Arecibo and Shigaraki, and *Nm*F2 and *hm*F2, observed by the ionospheric sounders agree with those generated by the 2-D time dependent model of the low-and middle-latitude ionosphere and plasmasphere of Pavlov (2003).

If the $\boldsymbol{E}\times\boldsymbol{B}$ plasma drift is directed from lower L-shells to higher L-shells, then a decrease in the $\boldsymbol{E}\times\boldsymbol{B}$ plasma drift leads to decreases in *Nm*F2 in the crest regions and to an increase in *Nm*F2 in the trough region, hampering the equatorial anomaly development, while a strengthening of this plasma drift causes an equatorial anomaly enhancement. A plasma drift due to wind transports plasma along magnetic field lines and causes changes in *Nm*F2 and in the crest-to-trough ratio of *Nm*F2 in the Northern and Southern Hemispheres, leading to a weakening or a strengthening of the equatorial anomaly. The value of *Nm*F2 is a function of [O], [N_2], and [O_2] at *hm*F2 at low geomagnetic latitudes (e.g. Pavlov et al., 2004b), and, therefore, storm-time changes in these number densities in one of the crest regions or in both crest regions or in the trough region contribute to changes in the equatorial anomaly development. As far as the authors know, the relative role of these mechanisms in the equatorial anomaly suppression is studied only by Pavlov et al. (2004b) for the 25–26 August 1987 geomagnetic storm. Pavlov et al. (2004b) found that weak differences between disturbed and quiet $\boldsymbol{E}\times\boldsymbol{B}$ plasma drifts cannot be responsible for the suppression of the equatorial anomaly on 26 August, and this suppression is due to the action of storm-time changes in neutral winds and densities on the equatorial anomaly development.

In this paper, we continue the study of the complex problem of the low-latitude ionospheric response to variations in the thermospheric wind, electric field, neutral composition, and neutral temperature during 17–22 March 1990 at solar maximum in the present case study, in which the electron density and temperature are measured simultaneously by the MU and Arecibo radars, and *Nm*F2 and *hm*F2 are observed by the Kokubunji, Yamagawa, Okinawa, Manila, Vanimo,

and Darwin ionospheric sounders. The use of data from the MU radar and the Arecibo radar, in combination with the ionosonde measurements, allows us to investigate the differences and similarities between the storm effects in the ionosphere in the different longitude sectors at low geomagnetic latitudes.

It has been well established that the F2-peak electron density shows anomalous nighttime enhancements under various geophysical conditions (see Pavlov and Pavlova, 2005a, and references therein). Many theories have been put forward to explain these nighttime enhancements in *Nm*F2. The mechanism which can account for the observed nighttime *Nm*F2 enhancements at middle geomagnetic latitudes is a combination of the plasmaspheric heating and refilling, and chemical and plasma transport effects (Pavlov and Pavlova, 2005a). The observed features of the nighttime enhancements in the total ionospheric electron content, TEC, at low geomagnetic latitudes, were reported by various workers (e.g. Young et al., 1970; Nelson and Cogger, 1971; Lanzerotti et al., 1975; Tyagi et al., 1982; Balan et al., 1994; Su et al., 1994; Jain et al., 1995; Unnikrishnan et al., 2002). The post-sunset enhancements in TEC and *Nm*F2 of the low-latitude ionosphere during geomagnetically quiet conditions were studied by Anderson and Klobuchar (1983), Dasgupta et al. (1985), Balan et al. (1995), and Su et al. (1995, 1997), using theoretical modeling techniques. Anderson and Klobuchar (1983) and Dasgupta et al. (1985) have shown that the prereversal increase of the meridional component of the $\boldsymbol{E}\times\boldsymbol{B}$ drift velocity primarily determines the development of the post-sunset enhancements in TEC near the crests of the equatorial anomaly. Seasonal, solar activity and latitude variations of the post-sunset enhancements in TEC and *Nm*F2 in the 10–30° geomagnetic latitude range at longitude 158° W were studied by Balan et al. (1995). The model calculations of Su et al. (1995), carried out for July at solar maximum, confirmed that the primary source for the nighttime enhancement in TEC at geomagnetic latitude 19° is the prereversal increase in the $\boldsymbol{E}\times\boldsymbol{B}$ plasma drift. It is shown by Su et al. (1997) that the difference in time of occurrence between the peak value of the prereversal increase in the $\boldsymbol{E}\times\boldsymbol{B}$ plasma drift and in the peak values of TEC and *Nm*F2 at equinox under solar maximum conditions at the crests of the equatorial anomaly varies with longitude because of the longitudinal difference of the neutral wind.

In this paper, we present the first theoretical study of the physical mechanisms responsible for electron density enhancements at night close to the geomagnetic equator, using the sounder low-latitude data during 17–22 March 1990 and a time-dependent two-dimensional model of the low- and middle-latitude ionosphere and plasmasphere described in Sect. 2.

$O^+(^4S)$ ions which dominate at ionospheric F2-region altitudes are lost in the reactions of $O^+(^4S)$ with unexcited $N_2(v=0)$ and $O_2(v=0)$ and vibrationally excited $N_2(v)$ and $O_2(v)$ molecules at vibrational levels, $v>0$. Vibrationally excited N_2 and O_2 react more strongly with $O^+(^4S)$ ions in comparison with unexcited N_2 and O_2 (Schmeltekopf et al., 1968; Hierl et al., 1997). As a result, an additional reduction in the electron density is caused by the reactions of $O^+(^4S)$ ions with vibrationally excited N_2 and O_2 (Pavlov, 1994; Richards et al., 1994b; Jenkins et al., 1997; Pavlov and Buonsanto, 1997; Pavlov and Oyama, 2000; Pavlov and Foster, 2001; Pavlov, 2003; Pavlov et al., 2004a, b). In this paper we examine the effects of vibrationally excited N_2 and O_2 on the electron density and temperature during 17–22 March 1990 and study, for the first time, the role of $N_2(v>0)$ and $O_2(v>0)$ in the equatorial anomaly development.

2 Theoretical model

The model of the low- and middle-latitude ionosphere and plasmasphere, which is described in detail by Pavlov (2003), calculates number densities, N_i, of $O^+(^4S)$, H^+, NO^+, O_2^+, N_2^+, $O^+(^2D)$, $O^+(^2P)$, $O^+(^4P)$, and $O^+(^2P^*)$ ions, the electron density, N_e, and temperature, T_e, and the ion temperature, T_i. The model includes the production and loss rates of ions by the photochemical reactions presented by Pavlov (2003) and Pavlov and Pavlova (2005b), except for the rate coefficient of the $O^+(^2D)$+O reaction, which is taken from Fox and Dalgarno (1985). The horizontal components of the neutral wind are specified using the HWM90 wind model (Hedin et al., 1991); the model solar EUV fluxes are produced by the EUVAC model (Richards et al., 1994a), while neutral densities and temperature are taken from the NRLMSISE-00 model (Picone et al., 2002).

The model calculations are carried out in dipole orthogonal curvilinear coordinates q, U, and Λ, where q is aligned with, and U and Λ are perpendicular to, $\boldsymbol{B}$, and the U and Λ coordinates are constant along a dipole magnetic field line. It should be noted that $q=(R_E/R)^2 \cos\Theta$, $U=(R_E/R)\sin^2\Theta$, and the value of Λ is the geomagnetic longitude, where R is the radial distance from the geomagnetic field center, $\Theta=90^0-\varphi$ is the geomagnetic colatitude, φ is the geomagnetic latitude, R_E is the Earth's radius.

The model takes into account that the $\boldsymbol{E}\times\boldsymbol{B}$ plasma drift velocity can be presented as $\boldsymbol{V}^E=V^E_\Lambda\,\boldsymbol{e}_\Lambda+V^E_U\,\boldsymbol{e}_U$, where $V^E_\Lambda=E_U/B$ is the zonal component of $\boldsymbol{V}^E$, $V^E_U=-E_\Lambda/B$ is the meridional component of $\boldsymbol{V}^E$, $\boldsymbol{E}=E_\Lambda\,\boldsymbol{e}_\Lambda+E_U\,\boldsymbol{e}_U$, E_Λ is the Λ (zonal) electric field in the dipole coordinate system, E_U is the U (meridional) component of $\boldsymbol{E}$ in the dipole coordinate system, $\boldsymbol{e}_\Lambda$ and $\boldsymbol{e}_U$ are unit vectors in Λ and U directions, respectively, $\boldsymbol{e}_U$ is directed downward at the geomagnetic equator. We use the implementation of the Eulerian-Lagrangian method developed by Pavlov (2003) in solving the time dependent and two-dimensional continuity and energy equations at a (q,U) plane. The combination of the Lagrangian and Euleurean approaches used consists mainly of two steps, an advection step and an interpolation step (Pavlov, 2003). The trajectory of the ionospheric plasma

Table 1. Ionosonde station and radar names and locations. Geomagnetic latitudes and longitudes of the ionosonde stations and radars are calculated on the surface of the Earth in the eccentric (first number) and centered (second number) dipole approximations for the geomagnetic field using the parameters of these magnetic field approximations for the time period 1990. The calculated L-shell values correspond to magnetic field lines which intersect 300-km altitude over the sounders and radars, the eccentric (first number) and centered (second number) dipole approximations are used.

Ionosonde station and radar names	Geographic latitude	Geographic longitude	Geomagnetic latitude	Geomagnetic longitude	L
Kokubunji	35.7	139.5	27.4, 26.2	206.7, 207.5	1.228, 1.300
Yamagawa	31.2	130.6	21.7, 21.0	198.5, 199.8	1.124, 1.202
Okinawa	26.3	127.8	16.2, 16.0	196.1, 197.6	1.052, 1.133
Manila	14.6	121.1	3.2, 4.0	189.9, 191.9	0.977, 1.052
Vanimo	–2.7	141.3	–13.9, –11.8	213.0, 213.2	1.033, 1.093
Darwin	–12.45	130.95	–25.3, –22.5	202.3, 203.4	1.199, 1.226
MU radar	34.85	136.10	26.1, 25.1	203.5, 204.5	1.202, 1.276
Arecibo radar	18.35	293.25	26.5, 29.2	7.2, 4.8	1.377, 1.373

perpendicular to magnetic field lines and the moving coordinate system are determined from equations derived by Pavlov (2003). The effects of the zonal (geomagnetic east-geomagnetic west) component of the $\boldsymbol{E}\times\boldsymbol{B}$ drift on N_e, N_i, T_e, and T_i are not taken into consideration because it is believed (Anderson, 1981) that these effects are negligible. As a result, the model works as a time dependent, 2-D (q and U coordinates) model of the ionosphere and plasmasphere. In this approximation, time variations of U, caused by the existence of the zonal electric field, are determined by time variations of the effective zonal electric field, $E_\Lambda^{\rm eff}=E_\Lambda RR_E^{-1}\sin\Theta$, and the value of $E_\Lambda^{\rm eff}$ is not changed along a magnetic field line (Pavlov, 2003).

Pavlov (2003) and Pavlov et al. (2004 a, b) used a mathematical model of the ionosphere and plasmasphere which incorporated a centered tilted magnetic dipole representation for the geomagnetic field and employed the averaged parameters (Akasofu and Chapman, 1972) of the centered tilted magnetic dipole, whose magnetic moment is located in the Earth's center and is inclined with respect to the Earth's rotational axis (the first three coefficients in the expansion of the geomagnetic field potential are taken into consideration in this approach). In the updated model of the ionosphere and plasmasphere, the Earth's magnetic field is approximated by the field of the eccentric tilted magnetic dipole, whose magnetic moment is inclined with respect to the Earth's rotational axis but is located at a point which is not coincided with the Earth's center (the first eight nonzero coefficients in the expansion of the geomagnetic field potential in terms of spherical harmonics are taken into account). The dependences of the parameters of the eccentric tilted magnetic dipole on a year are given by Frazer-Smith (1987) and Deminov and Fishchuk (2000).

The model calculates the values of N_i, N_e, T_i, and T_e in the fixed nodes of the fixed volume grid. This Eulerian computational grid consists of a distribution of the dipole magnetic field lines in the ionosphere and plasmasphere. One hundred dipole magnetic field lines are used in the model for each fixed value of Λ. The number of the fixed nodes taken along each magnetic field line is 191. For each fixed value of Λ, the region of study is a (q, U) plane, which is bounded by two dipole magnetic field lines. The computational grid dipole magnetic field lines are distributed between the low and upper boundary lines. Each computational grid dipole magnetic field line intersects the geomagnetic equatorial point (q=0) at the geomagnetic equatorial crossing height $h_{eq}^k=h_{eq}^1+\Delta h_{eq}^1+\ldots+\Delta h_{eq}^{kk}$, where k=1,...kk, kk=100, Δh_{eq}^k is the interval between neighboring computational grid lines. In the model, the low boundary magnetic field line intersects the geomagnetic equatorial point at the geomagnetic equatorial crossing height h_{eq}^1=150 km. The computational grid lines have the interval Δh_{eq}^k of 20 km for k=1 and 2, and the value of Δh_{eq}^k is increased from 20 km to 42 km linearly, if the value of k is changed from k=2 to k=kk. The upper boundary magnetic field line has h_{eq}^{kk}=4264 km.

In this work, we use data from the MU and Arecibo radars and from the Kokubunji, Yamagawa, Okinawa, Manila, Vanimo, and Darwin ionospheric sounders (see Sect. 3), whose locations are shown in Table 1. It follows from Table 1 that the sounders and the MU radar are located within $\pm11.55^\circ$ geomagnetic longitude of one another, if the eccentric tilted magnetic dipole representation for the geomagnetic field is used. As a result, the model simulations are carried out in the (q, U) plane of 201.45° geomagnetic longitude, to compare the model results with the MU radar and sounder measurements. If the eccentric tilted magnetic dipole approximation for the geomagnetic field is applied, then the Arecibo radar is located in the (q, U) plane of 7.2° geomagnetic longitude, where the model simulations are carried out separately. If the geomagnetic field is represented by the eccentric tilted

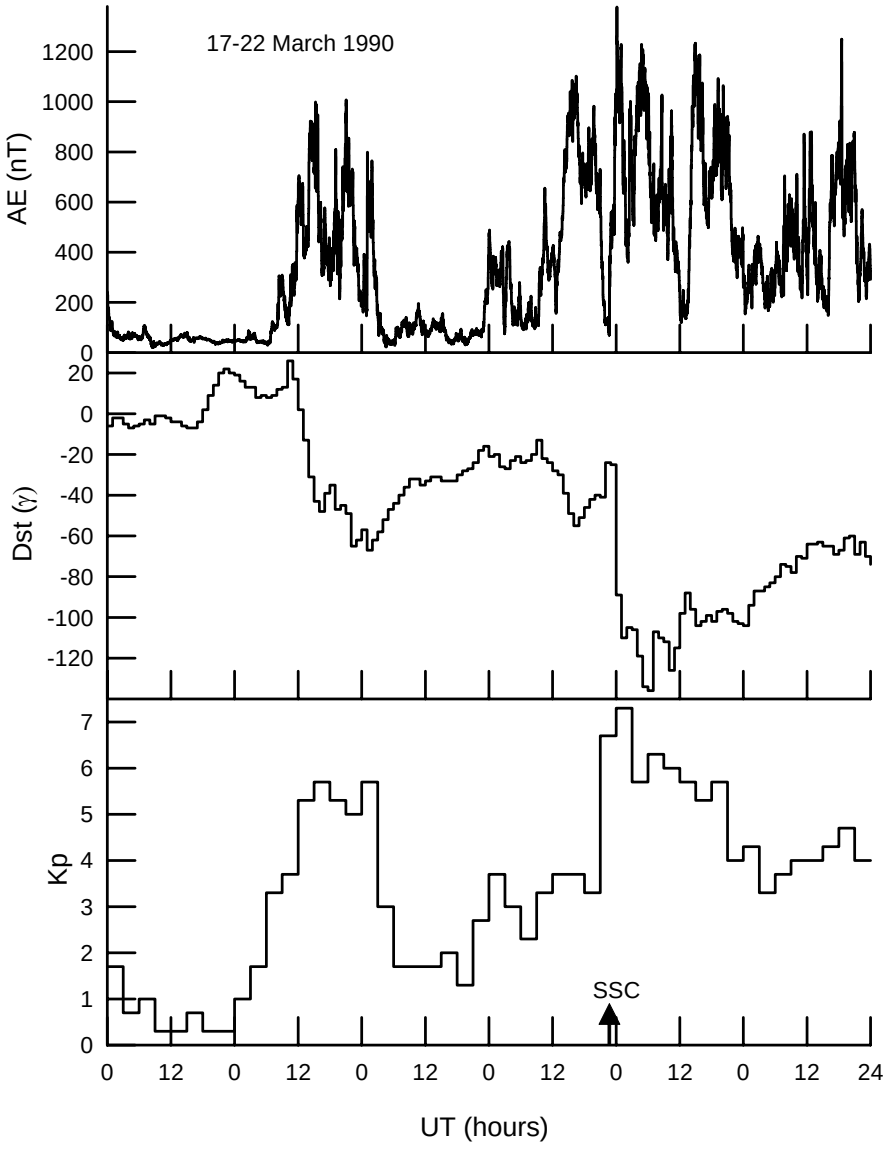

Fig. 1. The variation in the AE index (top panel), the Dst index (middle panel), and Kp index (bottom panel) during 17–22 March 1990. The SSC onset of the second geomagnetic storm is shown by the arrow in the bottom panel.

magnetic dipole, then the L-shell value of the upper boundary magnetic field line is equal to 1.592 and 1.738 for the (q, U) plane of 201.45° geomagnetic longitude and for the Arecibo (q, U) plane, respectively.

The empirical model of the storm-time vertical drift velocity of Fejer and Scherliess (1997) is used to determine E_{Λ}^{eff} at the equatorial dipole magnetic field lines which intersect the geomagnetic equatorial points at the geomagnetic equatorial crossing heights $h_{eq}^{k} \leq 600$ km. The value of E_{Λ}, which corresponds to the plasma drift velocity, is corrected in order to bring the measured and modelled F2-region peak altitudes into better agreement (see Sect. 4.1.1). This corrected equatorial zonal electric field is considered as the disturbed equatorial zonal electric field for the studied time period.

There are no MU radar vertical drift velocity measurements for the period under investigation. We take into account that the perpendicular drifts over Arecibo and the MU radar are similar for the same local time (Takami et al., 1996). Let us us L_A as the McIlwain parameter of the geomagnetic field line, which corresponds to the Arecibo radar. The average time zonal electric field derived from Arecibo radar scatter observations, appropriate for a high level of solar activity, is determined from the corresponding average $\boldsymbol{E}\times\boldsymbol{B}$ drift given by Fig. 2 of Fejer (1993). In the absence of measurements and an empirical model of a zonal electric field for the studied time period at F2-region altitudes for magnetic field lines which correspond to $L > L_A$, we suggest that the value of the effective zonal electric field is not changed at

300-km altitude for magnetic field lines at $L \geq L_A$. The effective equatorial zonal electric field is assumed to be the same at the geomagnetic equator for equatorial magnetic field lines with $h^k_{eq} < 600$ km. A linear interpolation between the equatorial and Arecibo values of the effective zonal electric field is employed at intermediate dipole magnetic field lines. The value of the zonal electric field is corrected to make the measured and modeled F2-region peak altitudes agree during the studied time period (see Sect. 4).

In the (q, U) plane of 201.45° geomagnetic longitude, the model starts at 05:13 UT on 15 March. This UT corresponds to 14:00 SLT (solar local time) at the geomagnetic equator and 201.45° of the geomagnetic longitude (SLT=UT+ψ/15, where ψ is the geographic latitude). The model is run from 05:13 UT on 15 March 1990 to 24:00 UT on 16 March 1990 before model results are used. The model starts at 18:24 UT on 17 March in the Arecibo (q, U) plane. This UT corresponds to 14:00 SLT at the geomagnetic equator and 7.2° of the geomagnetic longitude. The model is run from 18:24 UT on 17 March 1990 to 24:00 UT on 19 March 1990 before model results are used. We expect our finite-difference algorithm, which is described below, to yield approximations to N_i, N_e, T_i, and T_e in the ionosphere and plasmasphere at discrete times t=0, Δt, 2Δt, and so on up to the final discrete time with the time step Δt=10 min.

3 Solar geophysical conditions and data

The geomagnetically quiet conditions of 17 March 1990 (the geomagnetic activity index Ap changes from 3 to 8) and the 18–22 March 1990 magnetic storm period (the value of Ap changes from 14 to 73) were periods which occurred at solar maximum, when the 10.7 solar flux varied between 182 on 17 March and 243 on 22 March. In Fig. 1, the geomagnetic activity indexes Kp (bottom panel), Dst (middle panel), and AE (top panel), taken by INTERNET from the database of the National Geophysical Data Center (Boulder, Colorado, are plotted versus universal time. It is seen from Fig. 1 that during the 18–22 March 1990 period two geomagnetic storms took place with a gradual commencement time near 04:00 UT on 18 March and with a sudden commencement time near 22:45 UT on 20 March.

Intense storms have minimum values of $Dst \leq -100$ nT (Gonzalez and Tsurutani, 1987), while the first studied storm reached the minimum value of Dst=–67 nT at 01:00 UT–02:00 UT on 19 March 1990, followed by the recovery phase of the storm. Thus, this storm can be classified as a moderate storm. The AE index of the first storm remained perturbed until about 02:50–03:00 UT on 19 March. The SSC onset of the second geomagnetic storm was at 22:43 UT on 21 March and is shown by the arrow in the bottom panel of Fig. 1. This storm has the minimum value of Dst=–136 nT at 06:00 UT–07:00 UT on 21 March 1990 followed by the recovery phase of the geomagnetic storm, and this storm can be classified as an intense storm. The Dst index remained at less than –60 nT from 00:00 UT on 21 March to 24:00 UT on 22 March. The Kp index reached its maximum value of 6_- at 15:00 UT–18:00 UT and on 18 March and at 00:00 UT–03:00 UT on 19 March during the moderate storm, while the Kp maximum value was 7_+ at 00:00 UT–03:00 UT on 22 March during the intense storm.

The MU radar operated from 11:52 LT on 19 March to 11:37 LT on 22 March. The capabilities of the radar for incoherent scatter observations have been described and compared with those of other incoherent scatter radars by Sato et al. (1989) and Fukao et al. (1990). Rishbeth and Fukao (1995) reviewed the MU radar studies of the ionosphere and thermosphere. The data that we use in this work are the measured time variations of altitude profiles of the electron density and temperature, and the ion temperature between 200 km and 600 km over the MU radar.

The Arecibo incoherent scatter radar operated during the period 14:29 UT on 19 March to 02:00 UT on 23 March 1990, obtaining data on electron density, and electron and ion temperature variations. The experimental sequences used contained a number of pointing directions, but this study will use data observed in a local mode, using a scan at elevation angles between 75 and 90°. The final analysed data set covers the 145 to 686-km altitude with approximately 37–38-km resolution. Data are accessed using the MADRIGAL database at the Millstone Hill Observatory website (http://www.haystack.mit.edu/madrigal), located at Massachusetts Institute of Technology's Haystack Observatory. The detailed description of the Arecibo radar experiment is given by Buonsanto et al. (1992) and Buonsanto and Foster (1993).

We use hourly critical frequencies, *fo*f2 and *fo*E, of the F2 and E-layers, and maximum usable frequency parameter, M(3000)F2, data from the Manila ionospheric sounder station available at the Ionospheric Digital Database of the National Geophysical Data Center, Boulder, Colorado. Hourly *fo*f2, M(3000)F2, and *fo*E ionospheric parameters measured by the Kokubunji, Yamagawa, and Okinawa sounders were obtained from the National Institute of Information and Communications Technology of Japan, while the Australian Government IPS Radio and Space Service was used to obtain these data by Internet for the Vanimo and Darwin ionosondes.

The locations of these ionospheric sounder stations and the location of the MU and Arecibo radars are shown in Table 1. The value of the peak density, *Nm*F2, of the F2 layer is related to the critical frequency *fo*f2 as $NmF2 = 1.24 \cdot 10^{10}\ foF2^2$, where the unit of *Nm*F2 is m^{-3}, the unit of *fo*f2 is MHz. In the absence of adequate *hm*F2 data, we use the relation between *hm*F2 and the values of M(3000)F2, *fo*f2, and *fo*E recommended by Dudeney (1983) from the comparison of different approaches as $hmF2 = 1490/[M(3000)F2 + \Delta M] - 176$, where $\Delta M = 0.253/(foF2/foE - 1.215) - 0.012$. If there are no *fo*E data, then it is suggested that $\Delta M = 0$, i.e. the *hm*F2

formula of Shimazaki (1955) is used. The reliability of *hm*F2 derived from the observed values of M(3000)F2, *fo*f2, and *fo*E by means of the Dudeney (1983) approach is also supported by the reasonable agreement between these values of *hm*F2 and those measured by the MU radar during the geomagnetically quiet conditions of 19–21 March 1988 (Pavlov et al., 2004a), and during the geomagnetic storm periods of 25–27 August 1987 (Pavlov et al., 2004b) and 19–22 March 1990 (see Fig. 6, which is explained in Sect. 4.1.1).

4 Model results and discussion

4.1 The (q, U) plane at geomagnetic longitude 201.45°

4.1.1 Model/data comparisons

The measured (squares and circles) and calculated (lines) *Nm*F2 and *hm*F2 are displayed in Figs. 3–5 for the period under investigation above the Darwin (two lower panels in Fig. 3), Vanimo (two upper panels in Fig. 3), Manila (Fig. 4), Okinawa (two lower panels in Fig. 5), and Yamagawa (two upper panels in Fig. 5) ionosonde stations. The two lower panels of Fig. 6 show *Nm*F2 and *hm*F2 measured by the Kokubunji ionosonde station (squares and circles) and MU radar (crosses), in comparison with the calculated (lines) *Nm*F2 and *hm*F2 over the MU radar, while the measured (crosses) and modeled (lines) electron and O^+ ion temperatures at the F2-region main peak altitude above the MU radar are presented in the two upper panels of Fig. 6. The relations between *hm*F2 and the values of M(3000)F2, *fo*f2, and *fo*E (see Sect. 3) are used to determine the values of *hm*F2 shown by squares and circles, when the measured values of *fo*E are acceptable and not acceptable, respectively, i.e. the magnitudes of *hm*F2 shown by circles in Figs. 3–6 are overestimated. The results obtained from the model using the combination of $E_\Lambda^{\rm eff}$, based on the uncorrected zonal disturbed equatorial electric field (given by the dashed line in the bottom panel of Fig. 2), the NRLMSISE-00 neutral temperature and densities, and the HWM90 wind, as the input model parameters, are shown by dashed lines in Figs. 3–6. Solid and dotted lines in Figs. 3–6 show the results given by the model with the corrected zonal equatorial electric field (given by the solid line in the bottom panel of Fig. 2), the corrected NRLMSISE-00 neutral densities, and the corrected neutral wind, when vibrationally excited $N_2(v>0)$ and $O_2(v>0)$ are included (solid lines) and not included (dotted lines) in the loss rate of $O^+(^4S)$ ions. The corrections of E_Λ and the NRLMSISE-00 and HWM90 model corrections used in the model simulations, shown by solid and dotted lines in Figs. 3–6, are explained below.

It is seen from the comparison between the corresponding solid lines and data in Figs. 3–6 that the use of the corrected NRLMSISE-00 neutral densities, the corrected meridional HWM90 wind, and the corrected zonal electric field brings the measured and modeled *Nm*F2, *hm*F2, T_e, and T_i into reasonable agreement, although there are some quantitative differences. The reasonable agreement between the measured and modeled T_e and T_i determines the reliability of the calculated T_e and T_i at other geomagnetic latitudes. It should be noted that the measured *hm*F2 presented in Figs. 3–6 show large fluctuations. The possible source of this scatter in *hm*F2 is the relationship between *hm*F2 and M(3000)F2 and ΔM (see Sect. 3), which determines *hm*F2 with errors. Furthermore, the ionosondes listed in Table 1 are not located at the geomagnetic longitude of 201.45°, which is used in the model calculations. This geomagnetic longitude displacement can explain a part of the disagreement between the modeled and measured *hm*F2, *Nm*F2, T_e, and T_i in Figs. 3–6. A part of these discrepancies is probably due to the uncertainties in the model inputs, such as E_Λ, the NRLMSIS-00 model densities and temperature, the neutral wind, EUV fluxes, chemical rate coefficients, and photoionization, photoabsorption and electron impact cross sections for N_2, O_2, and O.

It follows from Figs. 3–6 that the use of the uncorrected E_Λ and the original HWM90 wind and NRLMSISE-00 neutral temperature and densities as the input model parameters brings the measured (squares, circles and crosses) and modeled (dashed lines) *Nm*F2, *hm*F2, T_e, and T_i into disagreement.

The vertical equatorial drift shows significant variability in the magnitude (Fejer, 2002), and the significant day-to-day variability of the quiet plasma drift in events from a database of Jicamarca observations was demonstrated by Scherliess and Fejer (1999). The empirical models of Scherliess and Fejer (1999) and Fejer and Scherliess (1997) for quiet and geomagnetically storm-time periods were created by averaging a great deal of data to find the mean trends in noisy data and create smooth curves. As a result, the averaged vertical drifts produced by these empirical models can differ from the vertical drifts for the studied time period, and can be modified to bring the measured and modeled *Nm*F2 and *hm*F2 into reasonable agreement over the Manila, Vanimo, and Okinawa sounders.

The time variations of the zonal electric field used in the model calculations are presented in the bottom (geomagnetic equator) and top (Arecibo) panels of Fig. 2. The dashed line in the bottom panel of Fig. 2 shows the empirical F-region storm-time equatorial zonal electric field found from the empirical model of the vertical drift velocity of Fejer and Scherliess (1997). The empirical model of Scherliess and Fejer (1999) is used to determine the F-region geomagnetically quiet equatorial zonal electric field shown by the dotted line in the bottom panel of Fig. 2. By the use of the comparison between the measured and modeled values of *hm*F2 and *Nm*F2 over the Manila, Vanimo, and Okinawa sounders, the value of this quiet equatorial zonal electric field was decreased by a factor of 1.5 from 23:00 UT on 16 March to 08:30 UT on 17 March, by a factor of 2 from 8:30 UT to

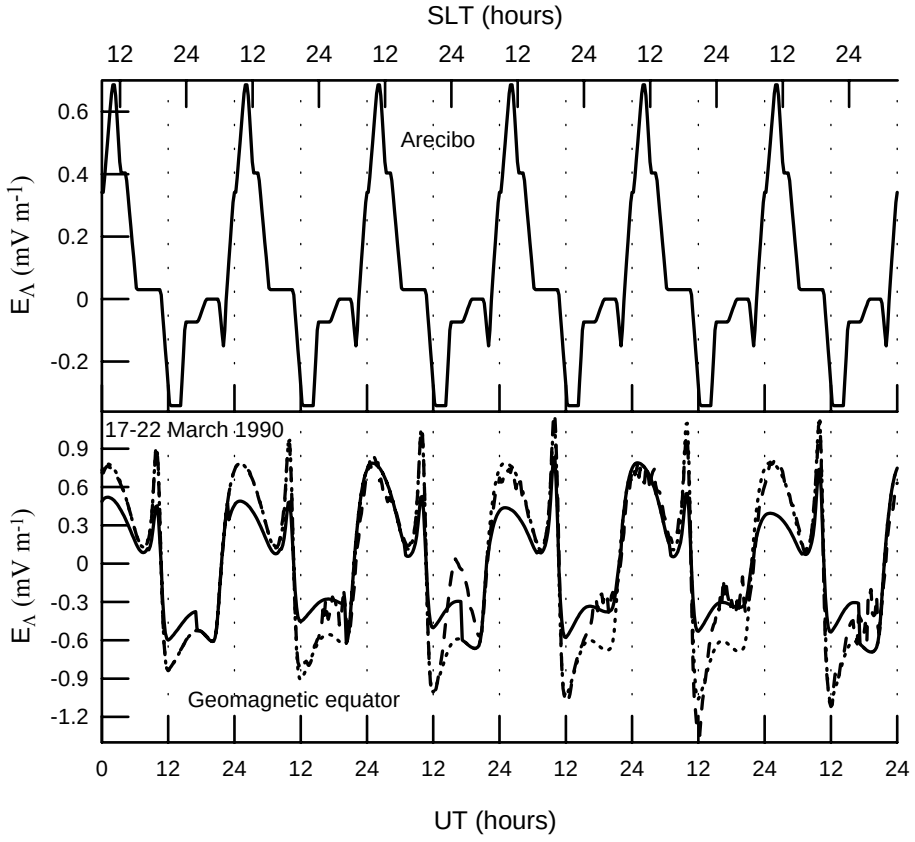

Fig. 2. Diurnal variations of the F-region zonal electric field during 17-21 March 1990 over the geomagnetic equator at 201.45° geomagnetic longitude (bottom panel) and over Arecibo (top panel). The zonal electric field at the F-region altitudes over Arecibo is found from Fig. 2 of Fejer (1993).The dashed line in the bottom panel show the storm-time equatorial zonal electric field found from the empirical model of Fejer and Scherliess (1997), while the geomagnetically quiet equatorial zonal electric field found from the empirical model of Scherliess and Fejer (1999) is presented by the dotted line in the bottom panel. The quiet equatorial zonal electric field is modified by the use of the comparison between the measured and modeled values of *hm*F2 and *Nm*F2 over the Manila, Vanimo, and Okinawa sounders (see Sect. 4.1) to produce the resulting storm-time equatorial zonal electric field shown by the solid line in the bottom panel. SLT is the local solar time at the geomagnetic equator and 201.45° geomagnetic longitude on the surface of the Earth.

11:00 UT on 17 March, by a factor of 1.4 from 11:00 UT to 17:00 UT on 17 March, by a factor of 1.6 from 23:00 UT on 17 March to 08:30 UT on 18 March, by a factor of 2 from 8:30 UT to 10:00 UT on 18 March, by a factor of 2 from 07:00 UT to 17:00 UT on 19 March, by a factor of 1.8 from 22:00 UT on 19 March to 07:00 UT on 20 March, by a factor of 1.3 from 07:00 UT to 10:45 UT on 20 March, by a factor of 1.8 from 10:45 UT to 22:00 UT on 20 March, by a factor of 2 from 07:00 UT on 21 March to 07:00 UT on 22 March, by a factor of 1.5 from 07:00 UT to 10:45 UT on 22 March, and by a factor of 2 from 10:45 UT to 17:00 UT on 22 March, to produce the resulting equatorial zonal electric field used in the model simulations and shown by the solid line in the bottom panel of Fig. 2.

As a result of the comparison between the modeled *Nm*F2 and *Nm*F2 measured by the ionosonde stations and by the MU radar, the NRLMSISE-00 model values of $[N_2]$ and $[O_2]$ were increased by a correction factor of C at all altitudes.

To bring the measured and modeled *Nm*F2 of the Northern Hemisphere into reasonable agreement, the value of C is found to be 1.5 above 16° geomagnetic latitude from 23:00 UT on 16 March to 20:00 UT on 17 March and from 22:00 UT on 17 March to 20:00 UT on 18 March, and its value decreases linearly from 1.5 to 1 in the 16° geomagnetic latitude range. We found that C=1.6 above 21° geomagnetic latitude from 03:00 UT to 12:00 UT on 19 March, and the $[N_2]$ and $[O_2]$ correction factor decreases linearly from 1.6 to 1.4 in the geomagnetic latitude range between 21° and 0°. The value of C is estimated from the numerical simulations to be 1.5 and 1.6 at geomagnetic latitudes exceeding 21° from 04:00 UT to 11:00 UT on 20 March and from 02:00 UT to 10:00 UT on 21 March, respectively, and this correction factor varies linearly from the above-mentioned values to 1 in the geomagnetic latitude range between 21° and 0°. In the time period from 21:00 UT on 21 March to 12:00 UT on 22 March, the $[N_2]$ and $[O_2]$ correction factor is found to

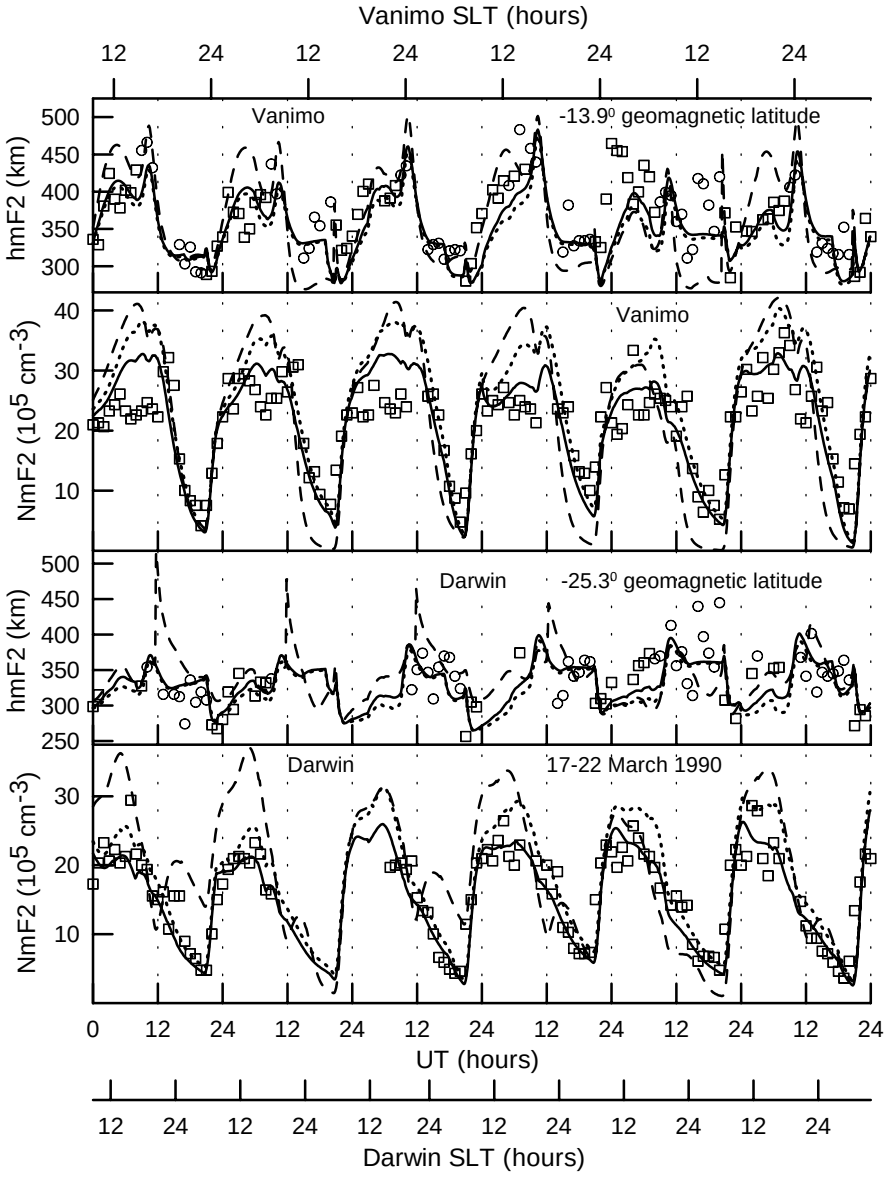

Fig. 3. Observed (squares and circles) and calculated (lines) *Nm*F2 and *hm*F2 above the Darwin (two lower panels) and Vanimo (two upper panels) ionosonde stations during 17–22 March 1990. The relations between *hm*F2 and the measured values of M(3000)F2, *fo*f2, and *fo*E (see Sect. 3) are used to determine the values of *hm*F2, when the measured values of *fo*E are acceptable (squares) and not acceptable (circles). The results obtained from the model of the ionosphere and plasmasphere, using E_{Λ}^{eff}, based on the uncorrected storm-time zonal electric field given by the dashed line in Fig. 2, the NRLMSISE-00 neutral temperature and densities, and the HWM90 wind as the input model parameters, are shown by the dashed lines. The solid lines show the results obtained from the model of the ionosphere and plasmasphere, using the combinations of E_{Λ}^{eff}, based on the corrected zonal electric field given by the solid line in Fig. 2, the corrected NRLMSISE-00 neutral densities, and the corrected neutral wind (see Sect. 4.1.1). The dotted lines show the results from the model with the same values of E_{Λ}^{eff}, the HWM90 wind, and the NRLMSISE-00 neutral densities, as for the solid lines, when vibrationally excited N_2 and O_2 are not included in the loss rate of $O^+(^4S)$ ions.

be 1.3 above 25° geomagnetic latitude; its value decreases linearly from 1.6 to 1.3 in the 16-25° geomagnetic latitude range, and a linear variation in the $[N_2]$ and $[O_2]$ correction factor from 1 to 1.6 is assumed in the geomagnetic latitude range between 0° and 16°.

The reasonable agreement between the measured and modeled *Nm*F2 is found if C=1.5 below –14° geomagnetic latitude from 23:00 UT on 16 March to 08:00 UT on 17 March and from 23:00 UT on 17 March to 06:00 UT on 18 March, and its value decreases linearly from 1.5 to 1 if

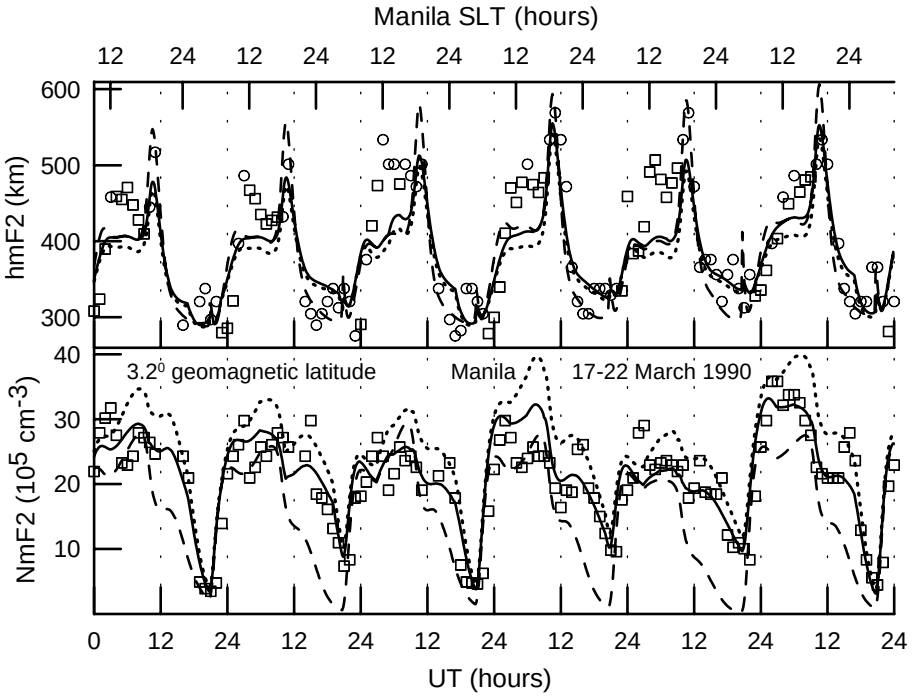

Fig. 4. Observed (squares and circles) and calculated (lines) *Nm*F2 (bottom panel) and *hm*F2 (top panel) above the Manila ionosonde station during 17–22 March 1990. The curves are the same as in Fig. 3.

the geomagnetic latitude is changed from –14° to 0°. The model simulations show that C=1.4 in the Southern Hemisphere from 03:00 UT to 12:00 UT on 19 March. In the time period from 00:00 UT to 13:00 UT on 20 March, the $[N_2]$ and $[O_2]$ correction factor is equal to 1.6 at –14° geomagnetic latitude, and its value decreases linearly from 1.6 to 1 if the geomagnetic latitude is changed from –14° to -25° and from –14° to 0°. The model uses the same value of C in the Southern Hemisphere in the time periods from 20:00 UT on 20 March to 07:00 UT on 21 March and from 22:00 UT on 21 March to 06:00 UT on 22 March. This value of C is found to be 1.2 below –25° geomagnetic latitude, the $[N_2]$ and $[O_2]$ correction factor is evaluated to be 1.4 at –14° geomagnetic latitude, and the value of C varies linearly from 1 to 1.4 and from 1.4 to 1.2 if the geomagnetic latitude is changed from 0° to –14° and from –14° to –25°, respectively.

Effects of the $\boldsymbol{E}\times\boldsymbol{B}$ plasma drift on *hm*F2 and *Nm*F2 over the Kokubunji and Darwin sounders and over the MU radar, whose locations are far enough from the geomagnetic equator, are much less than those caused by the plasma drift along magnetic field lines due to the neutral wind (Rishbeth, 2000; Souza et al., 2000; Pincheira et al., 2002; Pavlov, 2003; Pavlov et al., 2004a, b), and variations of *hm*F2 are predominantly determined by variations in the thermospheric wind over these sounders and the MU radar. The HWM90 wind velocities are known to differ from observations (Titheridge, 1995; Kawamura et al., 2000; Emmert et al., 2001; Fejer et al., 2002). The meridional, W, and the zonal components of the neutral wind are produced by the HWM90 wind model of Hedin et al. (1991) in geographical frame of reference, so that the meridional wind is directed northward for W>0 and southward for W<0. To bring the modeled and measured *hm*F2 and *Nm*F2 into reasonable agreement over the sounders shown in Table 1 and over the MU radar, the value of W taken from the HWM90 wind model is changed to W+ΔW. The value of ΔW shown in the Fig. 7 by the solid line is used above the geomagnetic latitude of 25° during 17–18 March and above the geomagnetic latitude of 21° during 19–22 March. The dashed line in Fig. 7 is the value of ΔW below the geomagnetic latitude of –14°, while ΔW=0 at the geomagnetic equator. A square interpolation of ΔW is employed between –14° and 0°, between 25° and 0°, and between 21° and 0° of the geomagnetic latitude, respectively.

4.1.2 Mechanism of nighttime enhancements in *Nm*F2 close to the geomagnetic equator

The most striking feature of the diurnal variations of the measured *Nm*F2 over Manila, shown in the bottom panel of Fig. 4, is the existence of the observed nighttime enhancements. Variations in neutral densities and temperature cannot be responsible for the enhanced ionization in the evening and night hours. Anomalous nighttime increases in *Nm*F2 cannot be explained in terms of traveling ionospheric disturbances, since these disturbances would have to be extremely large to produce the nighttime electron density observed (Young et

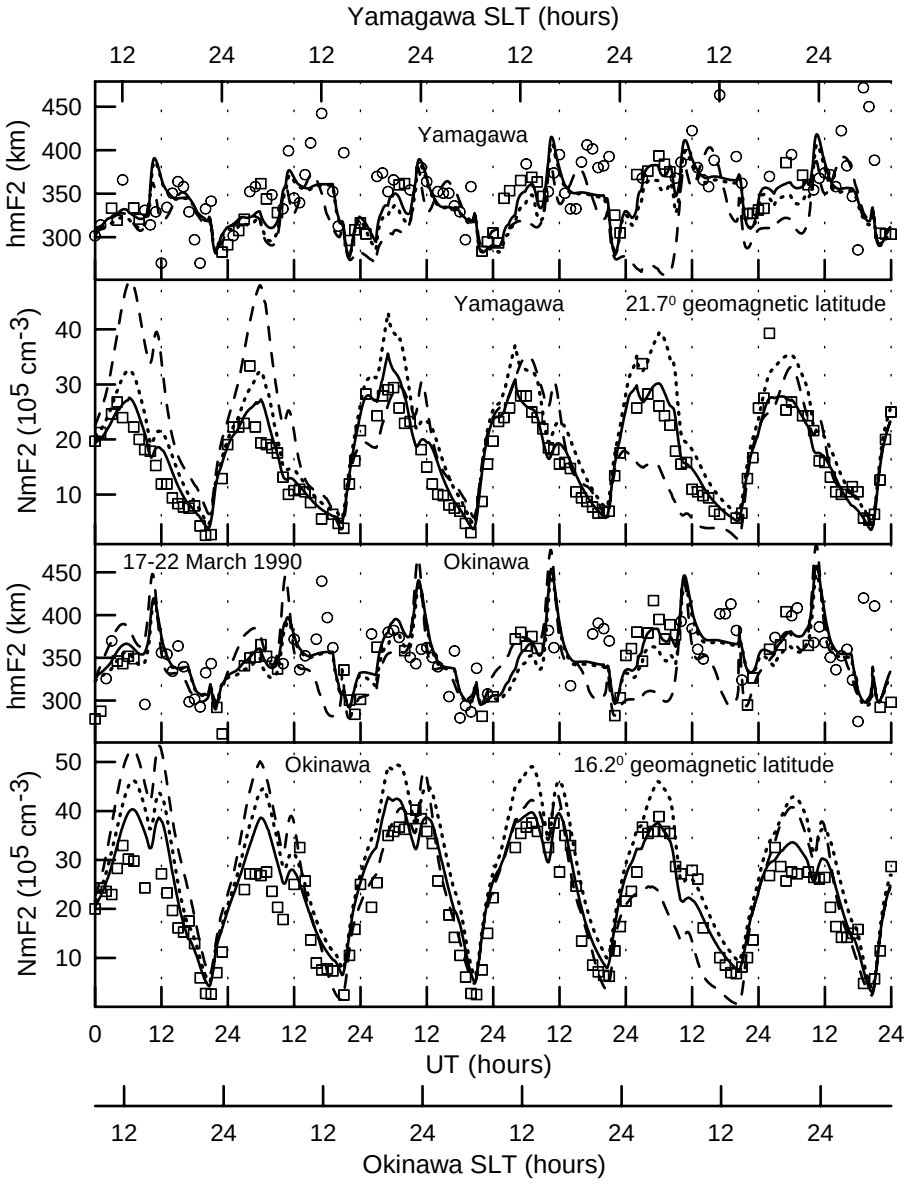

Fig. 5. Observed (squares and circles) and calculated (lines) *Nm*F2 and *hm*F2 above the Okinawa (two lower panels) and Yamagawa (two upper panels) ionosonde stations during 17–22 March 1990. The curves are the same as in Fig. 3.

al., 1970). The observed nighttime increases of *Nm*F2 can be explained by two mechanisms, first by an additional ionization process, and secondly by an influx of ions and electrons into the F2-region. At low geomagnetic latitudes, significant ionization of neutral components of the upper atmosphere by energetic particle is rather questionable. It is evident that the anomalous nighttime increases in *Nm*F2 observed over Manila during the geomagnetic quiet-time period of 17 March cannot be explained by the energetic electron precipitation. Furthermore, the Manila sounder is not located in a zone of a reduced geomagnetic field, where the enhancement of the energetic electron precipitation can be a source of additional ionization at F2-region altitudes (Pinto and Gonzalez, 1989). As a result, a flux of plasma into the nighttime F2-region, caused by the $\boldsymbol{E}\times\boldsymbol{B}$ drift, is considered as the plasma source to explain the enhancements in *Nm*F2 observed over Manila at night. It is worth noting that the plasma drift along magnetic field lines, due to neutral winds, can modulate the nighttime enhancements in *Nm*F2. A poleward meridional wind causes a lowering of the F2-region height and a resulting reduction in *Nm*F2, due to an increase in the loss rate of $O^+(^4S)$ ions, whereas a meridional wind, which is equatorwards, tends to increase the value of *Nm*F2 by transporting the plasma up along field lines to regions

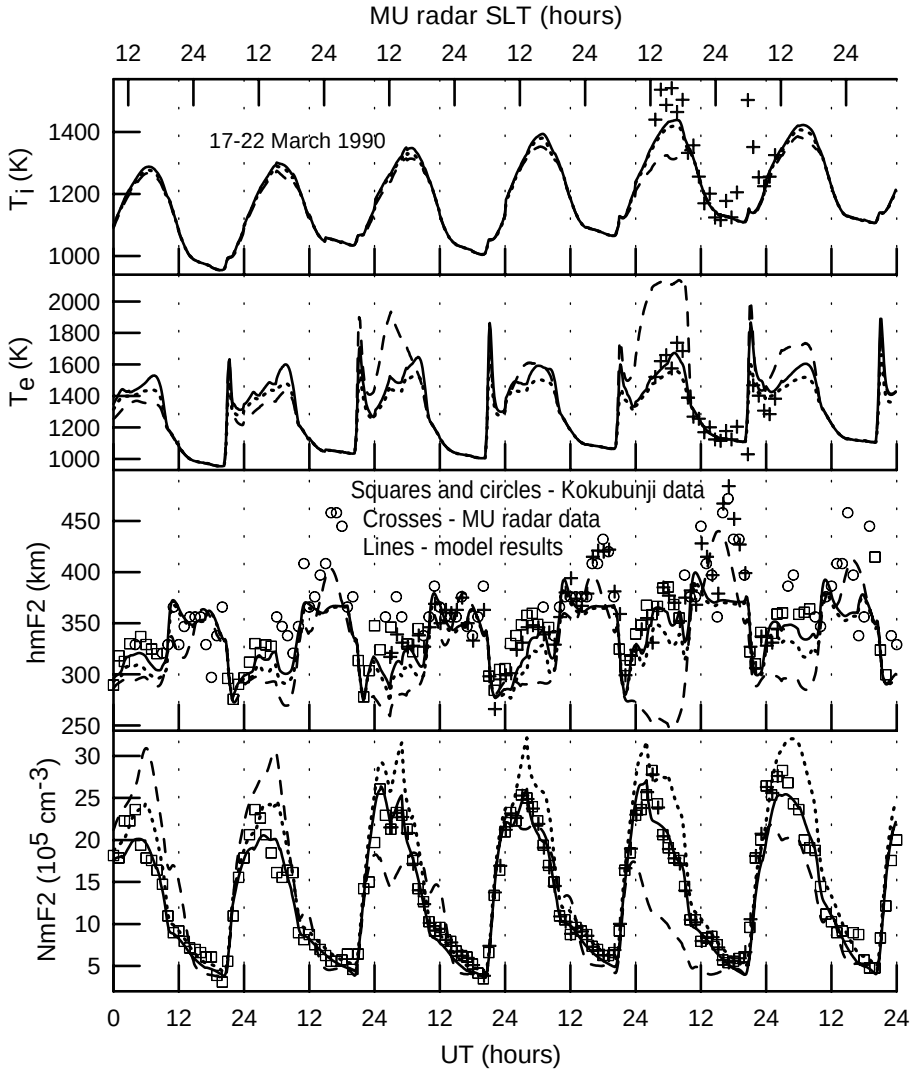

Fig. 6. Observed (crosses) and calculated (lines) *Nm*F2 and *hm*F2 (two lower panels), and electron and O^+ ion temperatures (two upper panels) at the F2-region main peak altitude above the MU radar during 17–22 March 1990. Squares and circles in the two lower panels show *Nm*F2 and *hm*F2 measured by the Kokubunji ionosonde. The relations between *hm*F2 and the measured values of M(3000)F2, *fo*f2, and *fo*E (see Sect. 3) are used to determine the values of *hm*F2, when the measured values of *fo*E are acceptable (squares) and not acceptable (circles). The curves are the same as in Fig. 3.

of lower chemical loss of $O^+(^4S)$ ions. The direction of the meridional neutral wind is, in general, poleward during day-time periods and equatorward at night at middle and low-latitudes (Rishbeth, 1967, 1975; Hernandez and Roble, 1984a, b). The maximum value of the equatorward neutral wind occurs during pre-midnight hours at low-latitudes (Krishna Murthy et al., 1990).

The model simulations show that the plasma drift caused by the neutral wind assists in the development of the post-sunset enhancement in *Nm*F2 close to the geomagnetic equator, if this wind is equatorward relative to the geomagnetic equator and strong enough during the studied nighttime periods. Figure 8 shows the values found of the latitude distributions of the meridional neutral wind used in the model simulations instead of the HWM90 meridional neutral wind from 10:00 UT to 17:00 UT on 17 March (solid line in the top panel), from 10:30 UT to 19:00 UT on 18 March (solid line in the top panel), from 09:00 UT to 17:00 UT on 19 March (dashed line in the top panel), from 09:00 UT to 20:00 UT on 20 March (solid line in the bottom panel), from 09:00 UT to 21:00 UT on 21 March (dashed line in the bottom panel), and from 09:00 UT to 17:00 UT on 22 March (dotted line in the bottom panel). For the sake of simplicity, the model of the ionosphere and plasmasphere uses zero zonal neutral wind for these nighttime periods. To give an example of changes in the meridional neutral wind, the diurnal

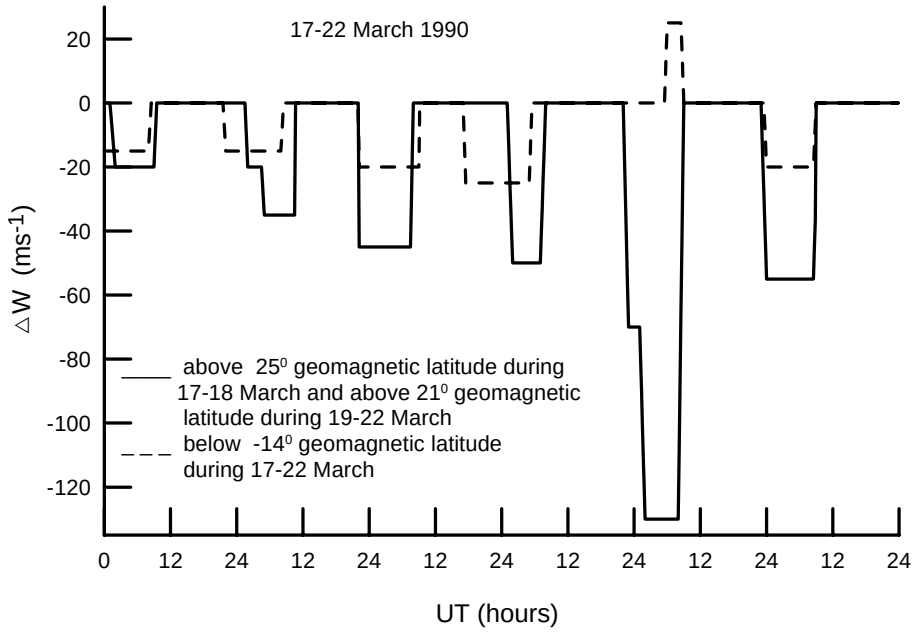

Fig. 7. Diurnal variations of the additional meridional neutral wind, ΔW, when the original value of the meridional HWW90 neutral wind, W, is changed to W+ΔW. The magnitude of ΔW is used in the Northern Hemisphere (solid line) above the geomagnetic latitude of 25° during 17–20 March and above the geomagnetic latitude of 21° during 19–22 March and in the Southern Hemisphere (dashed line) below the geomagnetic latitude of –14° during 17–22 March 1990, while ΔW=0 at the geomagnetic equator. A square interpolation of ΔW is employed between –14° and 0°, between 21° and 0°, and between 25° and 0° of the geomagnetic latitude, respectively.

variations of the modeled meridional uncorrected HWM90 neutral wind (dashed lines) and the modeled corrected meridional neutral wind (solid lines) are shown in Fig. 9 over the MU radar, and over the Okinawa, Manila, Vanimo, and Darwin ionosonde stations during 17–22 March 1990 at 300-km altitude. The corrected storm-time meridional wind found has nonregular variations in agreement with the early conclusions of Kawamura (2003)

The prereversal increase in the meridional component of the $\boldsymbol{E}\times\boldsymbol{B}$ drift velocity lifts the plasma from lower field lines to higher field lines. Simultaneously, the plasma diffuses along the magnetic field lines. These processes can support the development of the post-sunset enhancements in *Nm*F2 near the crests of the equatorial anomaly, decreasing *Nm*F2 close to the geomagnetic equator, i.e. the prereversal increase in the meridional component of the $\boldsymbol{E}\times\boldsymbol{B}$ drift velocity hampers the development of the post-sunset enhancements in *Nm*F2 near the geomagnetic equator.

The nocturnal, low-latitude F-region is maintained due to the low-latitude daytime F-region decay and by a diffusion of ions and electrons along magnetic field lines from the plasmasphere. In addition to these processes, the downward nighttime and morning $\boldsymbol{E}\times\boldsymbol{B}$ drift moves the plasma from middle to low geomagnetic latitudes, and ions and electrons then diffuse downward along the magnetic field lines. The resulting effect of the $\boldsymbol{E}\times\boldsymbol{B}$ drift on *Nm*F2 depends on the competition between an electron density enhancement caused by a plasma inflow and an electron density depletion due to an increase in the loss rate of $O^+(^4S)$ ions, owing to a *Nm*F2 peak layer lowering. It follows from the model simulations that the reduction in *Nm*F2 at night over Manila, caused by the increase in the loss rate of $O^+(^4S)$ ions, is stronger than the *Nm*F2 enhancement caused by the plasma outflow. The model calculations show that the value of the nighttime vertical equatorial plasma drift velocity, given by the empirical model of Fejer and Scherliess (1997) after the prereversal increase of the $\boldsymbol{E}\times\boldsymbol{B}$ drift, is excessively strengthened for the studied time period, preventing *Nm*F2 from the development of the post-sunset enhancements (see the dashed line in the bottom panel of Fig. 4). If the nighttime $\boldsymbol{E}\times\boldsymbol{B}$ drift produced by the empirical model of Fejer and Scherliess (1997) is weakened (compare the solid and dashed lines in the bottom panel of Fig. 2), then it causes an increase in *hm*F2, resulting in a decrease in the loss rate of $O^+(^4S)$ ions at *hm*F2 and leads to an increase in *Nm*F2 at night over the Manila sounder. On the other hand, a strong weakening of the nighttime $\boldsymbol{E}\times\boldsymbol{B}$ drift leads to a strong reduction of a plasma inflow, leading to a noticeable increase in *hm*F2 and a disagreement between the measured and modeled F2-layer peak altitudes. The corrected meridional $\boldsymbol{E}\times\boldsymbol{B}$ plasma drift and the plasma drift along magnetic field lines due to the corrected equatorward meridional neutral wind found from the model simulations produce the nighttime enhancements in *Nm*F2 observed over Manila.

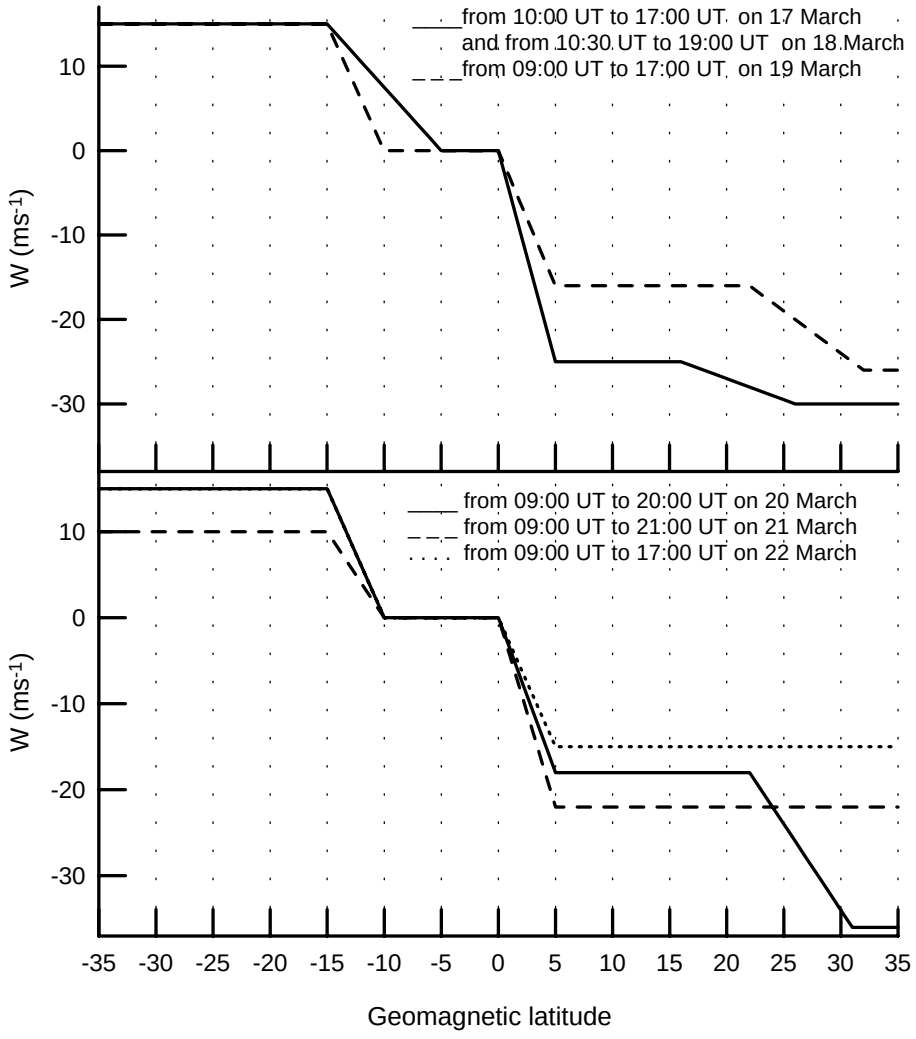

Fig. 8. The latitude distributions of the meridional neutral wind used in the model simulations instead of the HWM90 meridional neutral wind from 10:00 UT to 17:00 UT on 17 March (solid line in the top panel), from 10:30 UT to 19:00 UT on 18 March (solid line in the top panel), from 09:00 UT to 17:00 UT on 19 March (dashed line in the top panel), from 09:00 UT to 20:00 UT on 20 March (solid line in the bottom panel), from 09:00 UT to 21:00 UT on 21 March (dashed line in the bottom panel), and from 09:00 UT to 17:00 UT on 22 March (dotted line in the bottom panel).

The nighttime $\boldsymbol{E}\times\boldsymbol{B}$ drift of electrons and ions moves the plasma from higher L-shells to lower L-shells. As a result, changes in electron and ion densities caused by variations in the neutral wind at magnetic field lines, which do not intersect the studied F-region altitudes, lead to changes in the studied *hm*F2 and *Nm*F2. The model calculations show that the values of *hm*F2 and *Nm*F2 over Manila are practically not sensitive to variations in the nighttime, wind-induced plasma drift at magnetic field lines, which cross the geomagnetic equator above about 750 km height. In the (q, U) plane at the geomagnetic longitude of 189.9°, the magnetic field line passing through the geomagnetic equator at 750 km height crosses the 300-km altitude and the surface of the Earth at 15.3° and 19.75° geomagnetic latitude in the Northern Hemisphere and at –14.4° and –18.85° geomagnetic latitude in the Southern Hemisphere, respectively. The plasma drift, due to the neutral wind, which is equatorward relative to the geomagnetic equator in the both geomagnetic hemispheres, transports plasma along magnetic field lines, which are located between the above-mentioned geomagnetic latitudes, and contributes to the maintenance of the F2-layer observed over Manila at night during 17–22 March 1990.

Figure 10 shows diurnal variations of the modeled F2-region peak electron density (lines) over Vanimo (bottom panel), Manila (middle panel), and Okinawa (top panel) in comparison with the measured values of *Nm*F2 (squares). Solid lines show the results obtained from the model of the ionosphere and plasmasphere, using the combinations of $E_{\Lambda}^{\mathrm{eff}}$

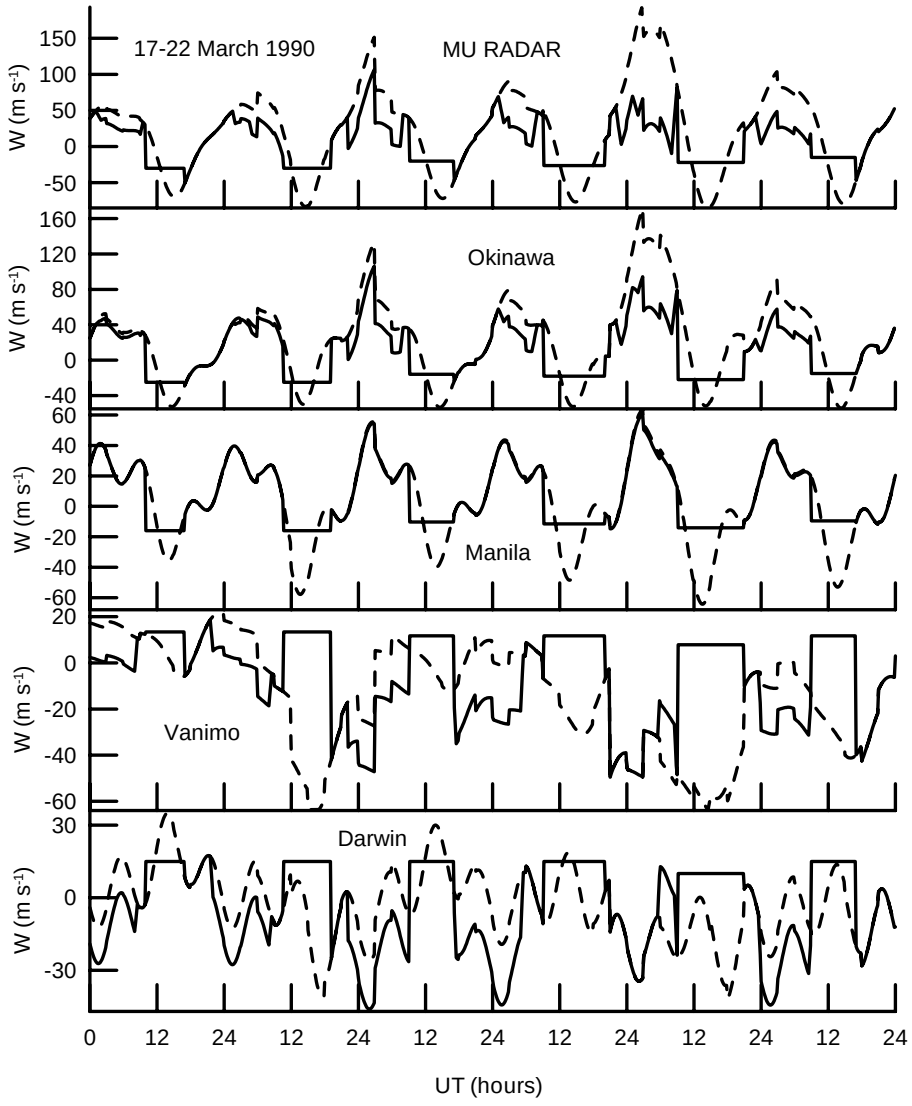

Fig. 9. Diurnal variations of the modeled meridional uncorrected (dashed lines) and corrected (solid lines) HWM90 neutral wind at 300 km altitude during 17–22 March 1990 over the MU radar, and over the Okinawa, Manila, Vanimo, and Darwin ionosonde stations. The meridional wind is directed northward for W>0 and southward for W<0 relative to the geographic equator.

based on the corrected zonal electric field given by the solid line in Fig. 2, the corrected NRLMSISE-00 neutral densities, and the corrected meridional wind. The original neutral HWM90 wind and the same values of the zonal electric field and the NRLMSISE-00 neutral densities as for the solid lines are used by the model to produce the results shown by the dashed lines. The results shown by dotted lines were calculated by the model which uses the original quiet vertical drift velocity of Scherliess and Fejer (1999) (dotted line in the bottom panel of Fig. 2) and the same corrections of the NRLMSISE-00 neutral densities and meridional neutral HWM90 wind as for the solid lines.

By comparing the corresponding solid and dotted lines in Fig. 10, it is seen that, close to the geomagnetic equator, the nighttime gain of ionization at the F2-peak, caused by the $\boldsymbol{E}\times\boldsymbol{B}$ drift, becomes greater that the loss of ionization arising from the lowering of *hm*F2 due to the nighttime weakening of E_Λ in comparison with that produced by the storm-time vertical drift velocity of Fejer and Scherliess (1997) or by the quiet vertical drift velocity of Scherliess and Fejer (1999). As a result, this weakening of E_Λ leads to the *Nm*F2 increase at night over the Manila sounder. The comparison of the model results presented by the solid and dotted lines in the middle panel of Fig. 10 indicates that this weakening of E_Λ cannot produce the nighttime enhancements in *Nm*F2 observed over Manila, if the original meridional HWM90 wind is used as the input parameter of the model of the ionosphere.

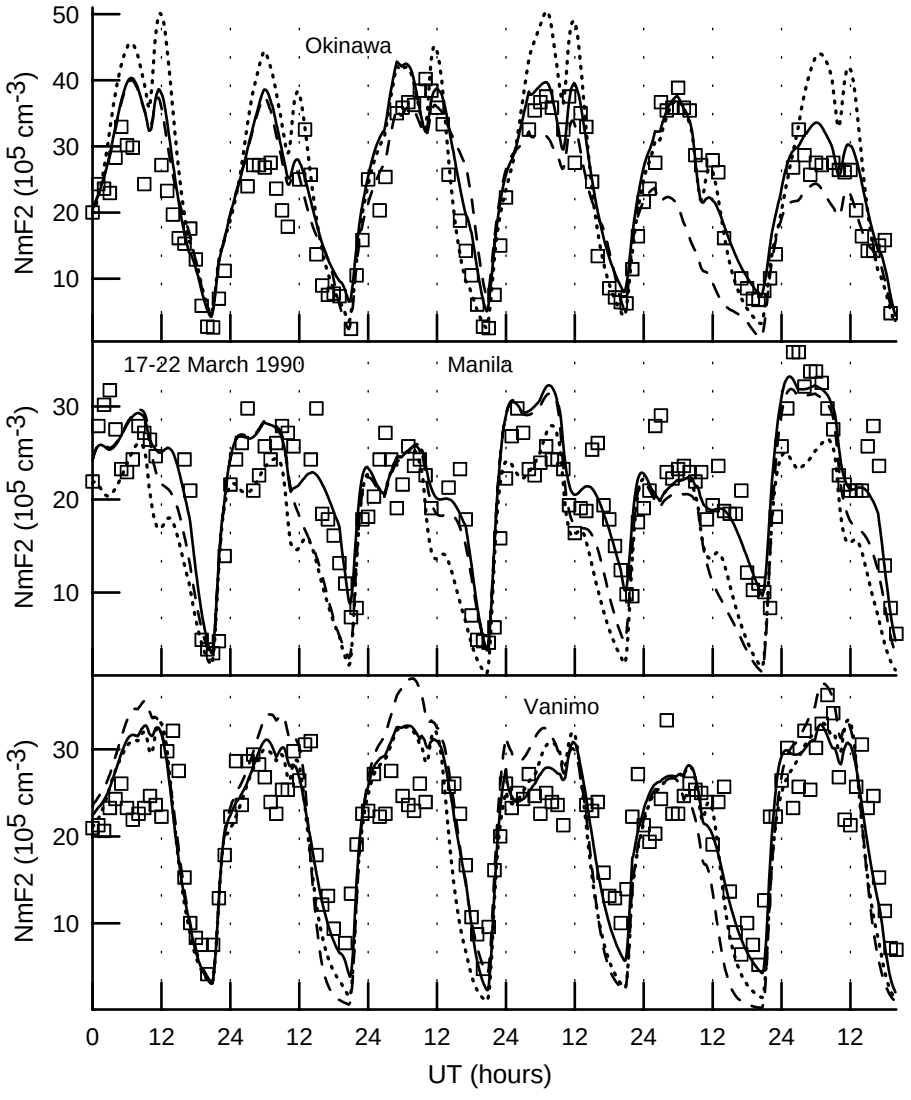

Fig. 10. Observed (squares) and calculated (lines) *Nm*F2 above the Vanimo (bottom panel), Manila (middle panel), and Okinawa (top panel) ionosonde stations during 17–22 March 1990. The dashed lines show the results produced by the model with the original neutral HWM90 wind and the same values of the zonal electric field and the NRLMSISE-00 neutral densities as for the solid lines. The results shown by the dotted lines were calculated by the model, which uses the original quiet vertical drift velocity of Scherliess and Fejer (1999) (dotted line in the bottom panel of Fig. 2) and the same corrections of the NRLMSISE-00 neutral densities and neutral wind as for the solid lines.

The second component of the new physical mechanism of the nighttime *Nm*F2 enhancement formation close to the geomagnetic equator, developed in this work, is the equatorward nighttime plasma drift along magnetic field lines caused by meridional neutral winds in the both hemispheres. By comparing squares and the dashed lines in Fig. 12, it can be seen that this equatorward wind-induced plasma drift alone cannot account for the observed nighttime peaks in *Nm*F2 over Manila. We conclude that the formation of the nighttime increases in *Nm*F2 observed over Manila during 22-26 April 1990 is explained by the above-mentioned weakening of the equatorial zonal electric field, combined with the equatorward plasma drift along magnetic field lines due to meridional neutral winds. It should be noted that a meridional neutral wind variability and a variability in the $\boldsymbol{E}\times\boldsymbol{B}$ plasma drift velocity can be responsible for the variability in time of the measured nighttime enhancements in *Nm*F2, which is not reproduced by the calculated F2-peak electron density.

4.1.3 Effects of vibrationally excited N_2 and O_2 on N_e, T_e, and T_i at *hm*F2

The importance of vibrationally excited N_2 and O_2 in controlling the behaviour of the low-latitude ionosphere is demonstrated by comparing the corresponding solid

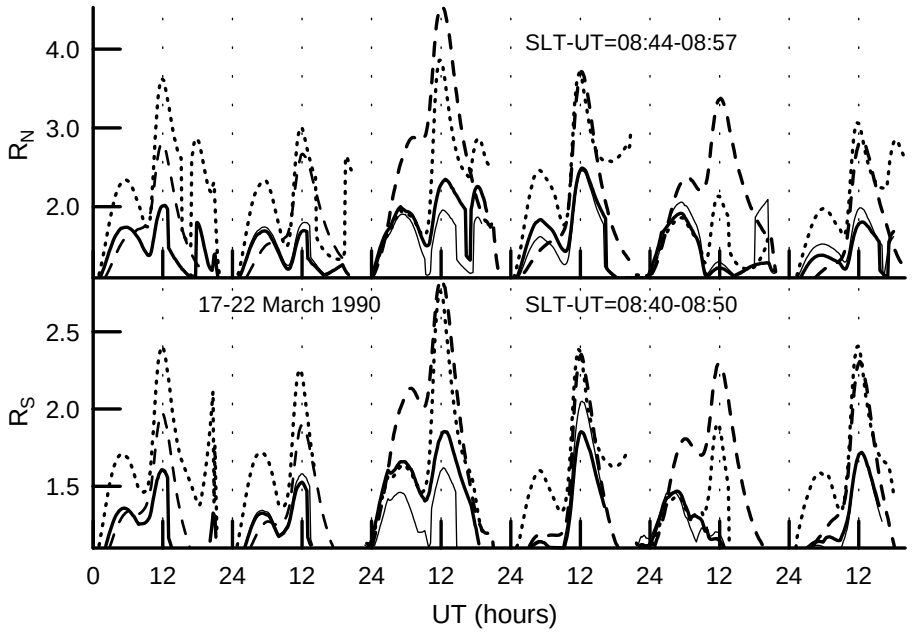

Fig. 11. The calculated crest-to-trough ratios in the northern (top panel) and southern (bottom panel) geomagnetic hemispheres during 17–22 March 1990. The heavy solid curves show the results obtained from the model of the ionosphere and plasmasphere, using the combinations of E_Λ^{eff}, based on the corrected zonal electric field given by the solid line in Fig. 2, the corrected NRLMSISE-00 neutral densities, and the corrected meridional wind. The dashed lines show the results produced by the model, using the combinations of E_Λ^{eff}, based on the corrected zonal electric field given by the solid lines in Fig. 2, zero neutral wind, and the NRLMSISE-00 neutral densities with the same corrections as for the heavy solid lines. The dotted lines show the results produced by the model, using the combinations of the E_Λ^{eff}, based on the geomagnetically quiet equatorial zonal electric field found from the empirical model of Scherliess and Fejer (1999) (dotted line in the bottom panel of Fig. 2), the HWM90 wind velocities with the same corrections as for the heavy solid lines, and the NRLMSISE-00 neutral densities with the same corrections as for the heavy solid lines. The thin solid lines show the results produced by the model using the same values of the zonal electric field and the neutral HWM90 wind as for the solid lines in Figs. 3–6, while neutral densities and temperature are taken from the NRLMSISE-00 model for hypothetical geomagnetically quiet conditions (seven 3-h geomagnetic indexes Ap are equal to 1), using the $[N_2]$ and $[O_2]$ correction factor found for the quiet day of 17 March for 17–22 March. The same values of a number of a given day and solar activity indexes as for the model results shown by the heavy solid, dashed and dotted lines are employed for the thin solid line. The differences between SLT and UT are 08:40–08:50 and 08:44–08:57 for model calculations of R_S and R_N, respectively.

(vibrationally excited N_2 and O_2 are included in the loss rate of $O^+(^4S)$ ions) and dotted (vibrationally excited N_2 and O_2 are not included in the loss rate of $O^+(^4S)$ ions) lines in Figs. 3–6. It follows from Figs. 3–6 that there are increases in the modeled *Nm*F2 and decreases in the calculated T_e at *hm*F2 if $N_2(v>0)$ and $O_2(v>0)$ are not included in the loss rate of $O^+(^4S)$ ions. The model simulations show that, in general, inclusion of $N_2(v>0)$ and $O_2(v>0)$ in the loss rate of $O^+(^4S)$ ions brings the modeled and measured *Nm*F2 into reasonable agreement. We found that, in the plane of the geomagnetic meridian at the geomagnetic longitude of 201.45°, the increase in the loss rate of $O^+(^4S)$ ions, due to $N_2(v>0)$ and $O_2(v>0)$, causes the maximum decrease in the calculated *Nm*F2 by a factor of 1.25, 1.26, 1.28, 1.33, 1.38, and 1.34 and the maximum change in the calculated *hm*F2 of 29, 16, 20, 20, 24, and 24 km in the low-latitude ionosphere over the ionosonde stations of Table 1 and over the MU radar on 17, 18, 19, 20, 21, and 22 March, respectively.

The effect of $N_2(v>0)$ and $O_2(v>0)$ on N_e changes the cooling rates of thermal electrons, causing the corresponding changes in T_e, and these changes of N_e and T_e produce the corresponding changes in T_i. As can be seen from the two upper panels of Fig. 6, the inclusion of $N_2(v>0)$ and $O_2(v>0)$ in the loss rate of $O^+(^4S)$ ions leads to increases in T_e and T_i. The model simulations show that the increase in the loss rate of $O^+(^4S)$ ions, due to vibrationally excited N_2 and O_2, causes the increase in T_e at *hm*F2 up to the maximum values of 239 K, 242 K, 285 K, 158 K, 350 K, and 268 K and the maximum increase in T_i of 17 K, 16 K, 21 K, 23 K, 23 K, and 26 K in the low-latitude ionosphere at *hm*F2 over the ionosonde stations of Table 1 and over the MU radar on 17, 18, 19, 20, 21, and 22 March, respectively.

4.2 Diurnal variations in the equatorial anomaly of *Nm*F2

The *Nm*F2 equatorial anomaly is characterized by a trough in the latitude distribution of *Nm*F2 near the geomagnetic

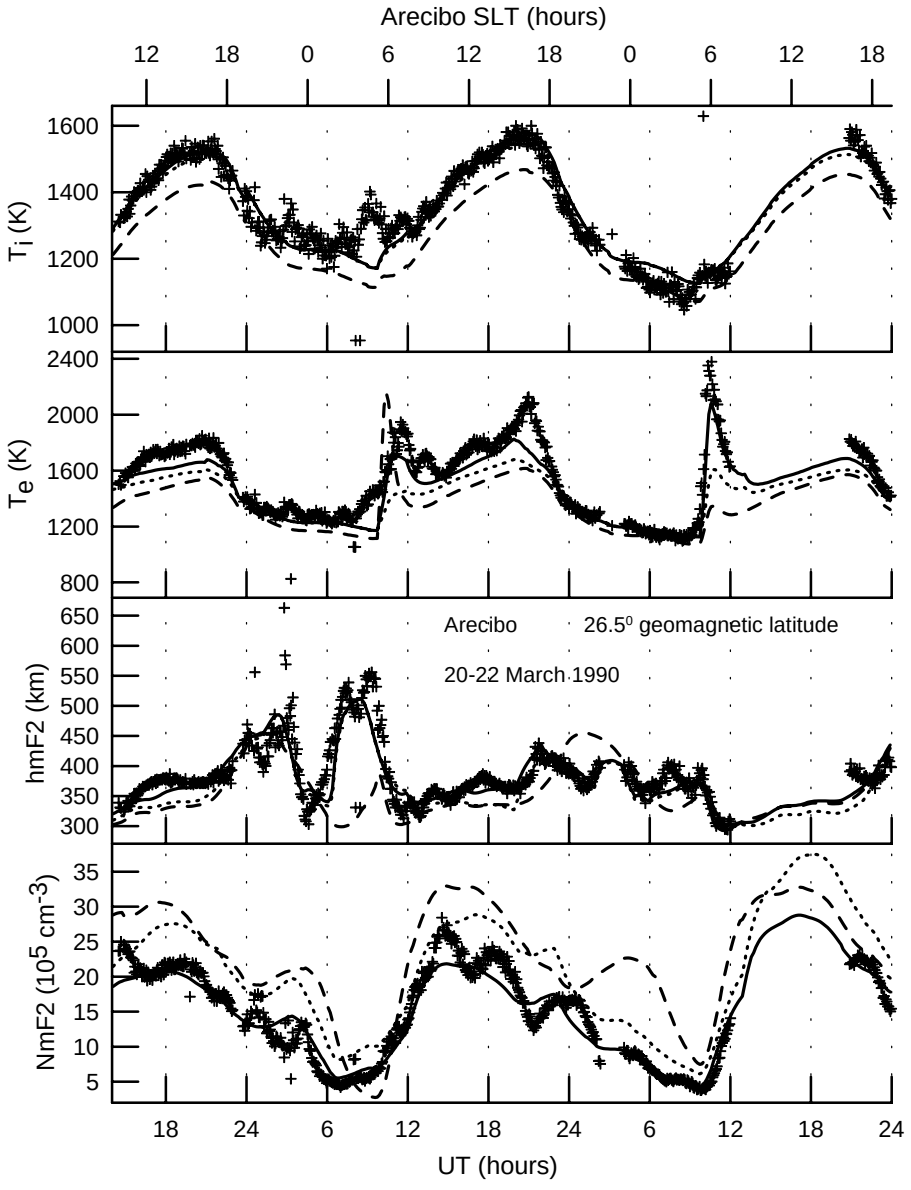

Fig. 12. Observed (crosses) and calculated (lines) *Nm*F2 and *hm*F2 (two lower panels), and electron and O^+ ion temperatures (two upper panels) at the F2-region main peak altitude above the Arecibo radar during 20–22 March 1990. SLT is the solar local time at the Arecibo radar. The results obtained from the model of the ionosphere and plasmasphere, using the original NRLMSISE-00 neutral temperature and densities and the original HWM90 wind as the input model parameters, are shown by dashed lines. Solid lines show the results produced by the model of the ionosphere and plasmasphere, using the corrected NRLMSISE-00 neutral temperature and densities, and the corrected meridional HWM90 wind (see Sect. 4.2). Dotted lines show the results from the model with the same values of the HWM90 wind and the NRLMSISE-00 neutral temperature and densities, as for solid lines, when vibrationally excited N_2 and O_2 are not included in the loss rate of $O^+(^4S)$ ions.

equator with southern and northern crests of *Nm*F2 and by the crest-to-trough ratios, R_N and R_S, for the Northern and Southern Hemispheres, respectively. For clarity sake, we believe in this work that the equatorial anomaly in *Nm*F2 is not distinguished if $R_N \leq 1.1$ and $R_S \leq 1.1$ at the same time.

Figure 11 shows the calculated crest-to-trough ratios in the northern (top panel) and southern (bottom panel) geomagnetic hemispheres during 17–22 March 1990. The combination of the model input parameters used in the calculations of the model results shown by the heavy solid lines in Fig. 11 is the same as that for the solid lines in Figs. 3–6. Zero neutral wind and the same values of the zonal electric field and the NRLMSISE-00 neutral densities as for the solid lines in Figs. 3–6 are used by the model to produce

Table 2. The maximum values of the crest-to-trough ratios, R_S^{max} and R_N^{max}, and their locations in UT and SLT, and the crest geomagnetic latitude at 201.45° geomagnetic longitude. Limits of variation of SLT are determined by SLT of the crest and SLT of the trough.

	Southern Hemisphere				Northern Hemisphere			
Day	UT	SLT	Geomagnetic latitude	R_S^{max}	UT	SLT	Geomagnetic latitude	R_N^{max}
17 March	11:50	20:34–20:41	–13	1.61	12:00	20:44–20:51	14	2.01
18 March	12:00	20:44–20:51	–12	1.53	12:20	21:04–21:11	13	1.70
19 March	12:40	21:24–21:32	–13	1.85	12:40	21:24–21:32	15	2.35
20 March	12:10	20:53–21:01	–13	1.85	12:20	21:09–21:14	14	2.49
21 March	04:40	13:23–13:33	–17	1.47	05:20	14:03–14:13	18	1.92
22 March	12:30	21:14–21:21	–12	1.72	12:40	21:24–21:31	13	1.81

the results shown by the dashed lines. The results shown by the dotted lines were calculated by the model which uses the original quiet vertical drift velocity of Scherliess and Fejer (1999) (dotted line in the bottom panel of Fig. 2) and the same corrections of the NRLMSISE-00 neutral densities and meridional neutral HWM90 wind as for the solid lines in Figs. 3–6. The thin solid lines show the results produced by the model using the same values of the zonal electric field and the neutral HWM90 wind as for the solid lines in Figs. 3–6, while neutral densities and temperature are taken from the NRLMSISE-00 model for hypothetical geomagnetically quiet conditions (seven 3-h geomagnetic indexes Ap are equal to 1), using the $[N_2]$ and $[O_2]$ correction factor found for the quiet day of 17 March for the 17–22 March period. The same values of a number of a given day and solar activity indexes as for the model results shown by the heavy solid lines and by the dashed and dotted lines in Fig. 11 are employed for the thin solid lines in Fig. 11.

It follows from the model simulations shown by the heavy solid lines in Fig. 11 that the model produces the distinguished equatorial anomaly in *Nm*F2, which is characterized by the both distinguished southern and northern crests ($R_N > 1.1$ and $R_S > 1.1$), from 02:10 UT to 13:40 UT and from 20:10 UT to 21:10 UT on 17 March, from 02:10 UT to 13:30 UT on 18 March, from 00:10 UT to 18:40 UT on 19 March, from 03:30 UT to 06:40 UT, and from 09:20 U to 16:20 UT on 20 March, from 23:40 UT on 20 March to 12:40 UT on 21 March, and from 03:10 UT to 15:30 UT on 22 March. The distinguished equatorial anomaly in *Nm*F2, which is characterized only by the distinguished northern crest ($R_S \leq 1.1$ and $R_N > 1.1$), occurs from 01:20 UT to 02:00 UT, from 13:50 UT to 20:00 UT, and from 21:20 to 21:30 UT on 17 March, from 01:10 UT to 02:00 UT and from 13:40 UT to 20:00 UT on 18 March, from 18:50 UT to 19:50 UT on 19 March, from 01:10 UT to 03:20 UT, from 06:50 UT to 09:10 UT, and from 16:30 to 22:00 UT on 20 March, from 12:50 UT to 19:30 UT on 21 March, from 02:00 UT to 03:00 UT and from 15:40 UT to 18:00 UT on 22 March. The equatorial anomaly in *Nm*F2 with both distinguished southern and northern crests is the longer-lasting phenomenon on 19 March than on 17, 18, 20, 21, and 22 March, and the shortest duration of the equatorial anomaly in *Nm*F2 occurs on 20 March. It is seen from Fig. 11 that the southern crest is more depleted than the northern crest during most of the studied time period. The calculated maximum values of the crest-to-trough ratios, R_S^{max} and R_N^{max}, and their time and geomagnetic latitude locations are shown in Table 2. It follows from Table 2 that the equatorial anomaly effect is most pronounced from 11:50 UT to 12:40 UT on 17, 18, 19, 20, and 22 March and from 04:40 UT to 05:20 UT on 21 March. If we determine a simple average maximum value of the crest-to-trough ratio as $<R_{max}> = 0.5\,(R_S^{max} + R_N^{max})$, then we find from Table 2 that the *Nm*F2 equatorial anomaly is less prominent in $<R_{max}>$ on 21 March than on 17, 18, 19, 20, and 22 March. The model simulations show that the latitudinal positions of the crests depend on the $\boldsymbol{E} \times \boldsymbol{B}$ drift velocity and on the neutral wind velocity during the studied time period.

The model simulations presented in Fig. 11 show that the equatorial plasma fountain, responsible for the equatorial anomaly formation, undergoes significant inhibition produced by meridional neutral winds, and by the difference in ΔE_Λ^* between the corrected equatorial zonal electric field used and that produced by the empirical model of Scherliess and Fejer (1999) for quiet conditions, and by geomagnetic storm disturbances in the neutral densities and temperature. By comparing the results of the calculations presented by the heavy solid lines with those shown by dashed, dotted, and thin solid lines in each panel of Fig. 11, we derive the conclusions about the relative role of these factors in the suppression or the development of the equatorial anomaly. It follows from Fig. 11 that during most of the studied time period, a total contribution from meridional neutral winds and ΔE_Λ^* to the equatorial anomaly changes is larger than that from geomagnetic storm disturbances in the neutral densities and temperature. The predominant source of the suppression of the equatorial anomaly is related to ΔE_Λ^* on 17, 18, 20 and 22 March and to the neutral wind circulation on 19 and

21 March. Our results show that geomagnetic storm disturbances in the neutral densities and temperature lead to either an enhancement or an inhibition of the equatorial anomaly.

It follows from the model simulations that if vibrationally excited N_2(v>0) and O_2(v>0) are not included in the loss rate of $O^+(^4S)$ ions ,then, during the predominant part of the studied time period, the calculated values of the crest-to-trough ratios are found to be less by about 10% than those produced by the model which includes vibrationally excited N_2(v>0) and O_2(v>0) in the loss rate of $O^+(^4S)$ ions. As a result, vibrationally excited N_2(v>0) and O_2(v>0) promote the equatorial anomaly enhancement during the predominant part of the studied time period, but the effect of vibrationally excited N_2(v>0) and O_2(v>0) on the development of the equatorial anomaly is not significant.

The model results show that the latitude variations of *hm*F2 and *Nm*F2 are asymmetrical about the geomagnetic equator, and comparison between heavy solid lines in the bottom and top panels of Fig. 11 provides evidence in favor of an asymmetry between the crest-to-trough ratios in the Northern and Southern Hemispheres. We conclude from the model calculations that the asymmetries in the neutral wind and in neutral densities relative to the geomagnetic equator are responsible for the north-south asymmetry in *Nm*F2 and *hm*F2, and for the asymmetry between the values of R_N and R_S.

4.3 The (q, U) plane at geomagnetic longitude 7.2° of Arecibo

There are no ionosonde and radar measurements of *Nm*F2 and *hm*F2 near the geomagnetic equator close to the geomagnetic longitude of 7° during the time period under investigation. As a result, we have no arguments to correct E_Λ from the comparison between the measured and modeled *hm*F2 and *Nm*F2, and the empirical model of the vertical drift velocity of Fejer and Scherliess (1997) is used to determine the F-region storm-time equatorial zonal electric field.

Shown in Fig. 12 are diurnal variations of the modeled (lines) and measured (crosses) F2-layer peak electron density and F2-layer peak altitude (two lower panels), and the electron and O^+ ion temperatures at the F2-region main peak altitude (two top panels) above Arecibo during 20–22 March 1990. Dashed lines are the variations in the ionospheric parameters obtained from the model of the ionosphere and plasmasphere using the NRLMSISE-00 neutral temperature and densities, and the HWM90 wind. The results produced by the model with the corrected NRLMSISE-00 neutral temperature and densities and the corrected neutral HWM90 wind are shown by solid and dotted lines, when vibrationally excited N_2(v>0) and O_2(v>0) are included (solid lines) and not included (dotted lines) in the loss rate of $O^+(^4S)$ ions. The NRLMSISE-00 and HWM90 model corrections used are explained below.

A comparison of the corresponding dashed lines and crosses in Fig. 12 shows considerable differences between the measured and modeled *Nm*F2, *hm*F2, and T_e and T_i at *hm*F2. In attempt to improve the agreement between the observed and modeled ionospheric parameters, the model calculations have been carried out using the corrected input parameters of the model of the ionosphere and plasmasphere.

By comparing the dashed line and crosses in the top panel of Fig. 12, it is seen that the measured ion temperature is higher than the calculated one. As a result, we infer that the disagreement between the measured and modeled ion temperature is caused by inaccuracies in the NRLMSISE-00 model prediction of the neutral temperature, T_n, for the studied geomagnetic storm-time period. To overcome the disagreement between the measured and modeled ion temperature, we multiply the value of T_n by the correction factor of 1.05 during the period under investigation.

We expect that the NRLMSISE-00 neutral model has some inadequacies in predicting the number densities with accuracy, and we have to change the number densities by correction factors at all altitudes, to bring the modeled electron densities into agreement with the measurements. As a result of the comparison between the modeled *Nm*F2 and *Nm*F2 measured by the Arecibo radar, the NRLMSISE-00 atomic oxygen density decrease of 30% was employed in the corrected model simulations at all altitudes from 12:00 UT on 20 March to 13:00 UT on 22 March. To bring the measured and modeled electron densities into agreement, the NRLMSISE-00 model values of $[N_2]$ and $[O_2]$ were increased by a factor of 2 at all altitudes from 22:00 UT on 20 March to 16:00 UT on 21 March, and by a factor of 1.5 from 23:00 UT on 21 March to 05:00 UT on 22 March.

The location of the Arecibo radar is enough far from the geomagnetic equator, and variations of *hm*F2 are predominantly determined by variations in the thermospheric wind above Arecibo (Bailey, 1980; Osterman et al., 1994; MacPherson et al., 1998). To bring the modeled and measured *hm*F2 and *Nm*F2 into reasonable agreement over Arecibo, the meridional neutral wind, W, taken from the HWM90 wind model, is changed to W+ΔW. The values of ΔW, shown in the low panel of Fig. 13, are used in the Northern Hemisphere above the geomagnetic latitude of 25°, while ΔW=0 at the geomagnetic equator. A square interpolation of ΔW is employed between 25° and 0° geomagnetic latitude.

The diurnal variations of the modeled meridional uncorrected HWM90 (dashed line) and corrected (solid line) meridional neutral wind over Arecibo during 20–22 March 1990 at 300-km altitude are shown in the top panel of Fig. 13. The model simulations predict the large equatorward meridional neutral wind of 108–127 ms^{-1} from 01:40 UT to 02:30 UT and 158-170 ms^{-1} from 06:30 UT to 08:30 UT on 21 March. It follows from the model simulations of *Nm*F2 and *hm*F2 presented in the two lower panels of Fig. 12 that such a large equatorward meridional wind velocity significantly affects *hm*F2 and *Nm*F2 over Arecibo, bringing the

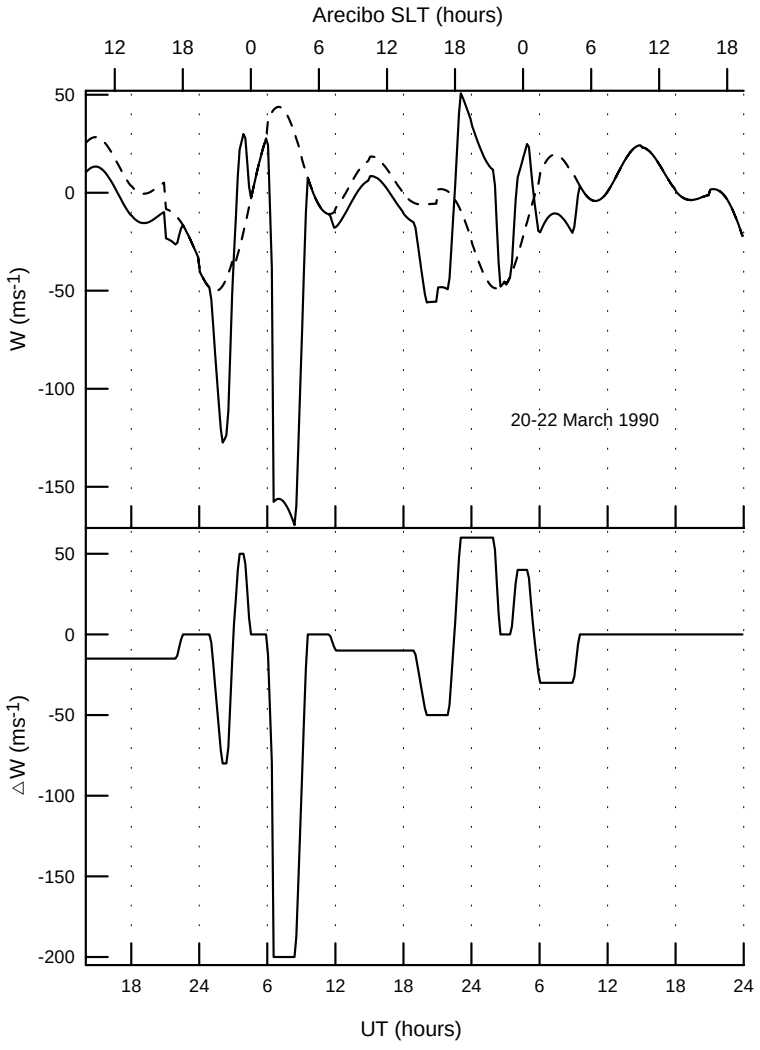

Fig. 13. Diurnal variations of the meridional neutral wind, W (top panel), and the additional meridional neutral wind, ΔW (bottom panel) during 20–22 March 1990 (when the original value of W is changed to W+ΔW). The values of ΔW are used in the Northern Hemisphere above the geomagnetic latitude of 25°, while ΔW=0 at the geomagnetic equator. A square interpolation of ΔW is employed between 25° and 0°. The modeled meridional corrected and uncorrected HWM90 meridional neutral winds at 300-km altitude over the MU radar are shown in the top panel by the solid and dashed lines, respectively. The meridional wind is directed northward for W>0 and southward for W<0.

measured and modeled *hm*F2 into reasonable agreement. A larger wind-induced equatorward plasma drift causes an even greater disparity between the measured and calculated F2-layer peak density, since this plasma drift raises the F2-layer into a region of lower loss rate of $O^+(^4S)$ ions, and the lower loss rate of $O^+(^4S)$ ions causes the F2-region to decay less rapidly until the meridional wind changes its own direction and becomes poleward. However, the comparison between the solid line and crosses in the bottom panel of Fig. 12 shows that the agreement between the measured and modeled *Nm*F2 is reasonable, if the correction of the NRLMSISE-00 model densities described above is used.

The Arecibo data between 270 and 430 km during the time period from 21:00 UT on 20 March to 12:00 UT on 21 March 1990 were used by Buonsanto and Foster (1993) to obtain the meridional neutral wind from the measured line-of-sight-velocities using two different techniques, which are called the no gradient method and the constant gradient method. These two different techniques lead to the noticeable difference between obtained neutral winds, underlining the possibility that during rapidly changing storm-time conditions results from neither technique may be valid (Buonsanto and Foster, 1993). The bottom panel of Fig. 5 of Buonsanto and Foster (1993) shows that the constant gradient technique results in a strong equatorward surge of about 220–230 ms^{-1} in

the meridional neutral wind close to 07:30 UT on 21 March. The largest meridional neutral wind surge derived in our paper from comparison between the modeled and measured F2-peak altitudes (see the solid line in the top panel of Fig. 13) is comparable to that of Buonsanto and Foster (1993).

The energy input during storm-time periods is mainly into the auroral regions, leading to a change in the global thermospheric wind circulation system. As a consequence of this high-latitude heating and expansion, equatorward directed neutral winds are generated which lift up the plasma along geomagnetic field lines. Equatorward storm-time meridional neutral winds are usually stronger at night, because an equatorward difference between a storm-time meridional wind and a geomagnetically quiet meridional wind adds to a geomagnetically quiet meridional neutral wind, which is usually equatorward at night (Titheridge, 1995). Figures 12 and 13 show that the striking increase in *hm*F2 following the F2-peak altitude decrease on 21 March is explained by the large equatorward surge of the meridional neutral wind. An equatorward wind surge is a result of an immediate thermospheric response to a storm energy input at high latitudes (Fuller-Rowell et al., 1994). Such storm-time wind surges extracted from *hm*F2 measured by the ionosondes in the South American region are reported by Pincheira et al. (2002). As a rule, an equatorward wind surge is a nighttime phenomenon as disturbance neutral winds caused by high-latitude heating are reinforced by the prevailing anti-sunward plasma convection at night, and neutral winds take the form of equatorward wind surges or traveling atmospheric disturbances when the high-latitude heating events are impulsive (Hocke and Schlegel, 1996; Buonsanto et al., 1999a; Buonsanto, 1999). The diurnal variations of the meridional neutral wind measured at the F2-region altitudes over Arecibo, including meridional wind surge events, were discussed by Friedman and Herrero (1982), Crary and Forbes (1986), Burnside and Tepley (1989), Burnside et al. (1991), Buonsanto and Foster (1993), Buonsanto et al. (1999a, b), MacPherson et al. (1998), and Pi et al. (2000). If the meridional neutral wind appears to be oscillating between sourthward and northward directions, then it implies possible gravity wave activity. The meridional wind behaviour at nighttime manifests itself through a maximum equatorward wind after midnight, suggesting a traveling atmospheric disturbance starting more earlier. Equatorward wind surges or traveling atmospheric disturbances may arise from both auroral zones, and large-scale gravity waves may propagate from high to low-latitudes, providing varying perturbations measured over Arecibo.

It follows from the top panel of Fig. 9 that there are no equatorward wind surges over the MU radar at 300-km altitude close to the time periods, when the large equatorward wind surges were found over Arecibo at 300-km altitude on 21 March. The large equatorward propagating surges of storm-time winds of limited longitude extension, derived from the model simulations, provide evidence in favor of an asymmetry in longitude of the energy input into the auroral regions of the Northern Hemisphere.

Solid lines in Fig. 12 represent the results obtained from the model with effects of vibrationally excited N_2 and O_2 on the $O^+(^4S)$ loss rate, while dotted lines in Fig. 12 show the model results when $N_2(v>0)$ and $O_2(v>0)$ are not included in the $O^+(^4S)$ loss rate. We find from the model calculations that the effects of $N_2(v>0)$ and $O_2(v>0)$ on T_i at *hm*F2 (though corresponding changes in N_e and T_e) are less than 27 K during 20–22 March 1990 and can be neglected. The increase in the loss rate of $O^+(^4S)$ ions, due to $N_2(v>0)$ and $O_2(v>0)$, leads to the maximum decrease in the calculated *Nm*F2 by factors of 1.36 (20 March), 1.51 (21 March), and 1.45 (22 March) and to the increase in the calculated electron temperature at *hm*F2 up to the maximum values of 74 K (20 March), 193 K (21 March), and 774 K (22 March), while the maximum change in the calculated F2-layer peak altitude of 24, 29, and 23 km, caused by $N_2(v>0)$ and $O_2(v>0)$ is found, from the model calculations over the Arecibo radar on 20, 21, and 22 March, respectively. As Fig. 12 shows, there is a large increase in the modeled *Nm*F2 without $N_2(v>0)$ and $O_2(v>0)$ in the $O^+(^4S)$ loss rate, and both the daytime and nighttime densities are not reproduced by the model. Including vibrationally excited N_2 and O_2 in the loss rate of $O^+(^4S)$ ions brings the measured and modeled electron densities into reasonable agreement and also tends to give reasonable agreement between the measured and modeled electron temperatures.

5 Conclusions

We have presented a comparison between the modeled *Nm*F2 and *hm*F2 and *Nm*F2 and *hm*F2 measured in the low-latitude ionosphere simultaneously by the Kokubunji, Yamagawa, Okinawa, Manila, Vanimo, and Darwin ionospheric sounders during the geomagnetically quiet-time period of 17 March 1990 and the 18–22 March 1990 geomagnetically storm-time period at solar maximum near approximately the same geomagnetic meridian of 201.45° in the Northern and Southern Hemispheres. A comparison between *Nm*F2, *hm*F2, and the electron and ion temperatures at *hm*F2, measured by the MU radar and those produced by the model of the ionosphere and plasmasphere, is given for the storm-time period of 19-22 March 1990. The values of *Nm*F2, *hm*F2, and the electron and ion temperature at *hm*F2, observed by the Arecibo radar, and the results of the model calculations over Arecibo are presented for the storm-time period of 20–22 March 1990, to compare the ionospheric storm-time variations in different longitude sectors. The corrections found in the zonal electric field, the meridional neutral wind taken from the HWM90 wind model, and the NRLMSISE-00 neutral temperature and densities, bring the model results and data into reasonable agreement.

Causes of the observed nighttime enhancement close to the geomagnetic equator observed over Manila following the rapid sunset decay are investigated, for the first time. We consider a flux of plasma into the nighttime F2-region, caused by the meridional component of the $\boldsymbol{E}\times\boldsymbol{B}$ drift, as the plasma source to explain the electron density enhancements observed over Manila at night. It is shown that the prereversal increase in the $\boldsymbol{E}\times\boldsymbol{B}$ drift velocity hampers the development of the post-sunset enhancements in *Nm*F2 near the geomagnetic equator. The weakening of this prereversal increase in the $\boldsymbol{E}\times\boldsymbol{B}$ drift in comparison with that given by the empirical models of the storm-time vertical drift velocity of Fejer and Scherliess (1997) or by the quiet vertical drift velocity of Scherliess and Fejer (1999) contributes to the *Nm*F2 nighttime increase. It is shown that the value of the nighttime vertical equatorial plasma drift velocity produced by these empirical models after the prereversal increase in the $\boldsymbol{E}\times\boldsymbol{B}$ drift is excessively strengthened for the studied nighttime periods preventing *Nm*F2 from the development of the post-sunset enhancements. If the nighttime plasma transport from higher L-shells to lower L-shells, produced by the $\boldsymbol{E}\times\boldsymbol{B}$ plasma drift, given by above-mentioned empirical models, is weakened, then it causes the *hm*F2 increase, resulting in the decrease in the loss rate of $O^+(^4S)$ ions at *hm*F2 and leads to the *Nm*F2 increase at night over the Manila sounder. We found that this weakening of the equatorial zonal electric field is not a sufficient condition to produce the observed nighttime enhancements in *Nm*F2, if the original meridional HWM90 wind is used as the input parameter of the model.

If the nighttime wind-induced plasma drift along magnetic field lines, which crosses a region close to *hm*F2 near the geomagnetic equator, is equatorward relative to the geomagnetic equator, then this plasma drift impedes the field-aligned downward plasma diffusion in both geomagnetic hemispheres causing, increases in electron and ion densities at F-region altitudes close to the geomagnetic equator. The nighttime $\boldsymbol{E}\times\boldsymbol{B}$ drift of electrons and ions moves the plasma from higher L-shells to lower L-shells and redistributes changes in electron and ion densities between field lines. As a result, variations in the neutral wind at magnetic field lines, which do not intersect the studied equatorial F-region altitudes, lead to changes in the studied *hm*F2 and *Nm*F2. The model simulations provide evidence that the corrected wind-induced plasma drift along magnetic field lines, which crosses the surface of the Earth equatorward of about 20° geomagnetic latitude in the Northern Hemisphere and about –19° geomagnetic latitude in the Southern Hemisphere, contributes to the maintenance of the F2-layer observed over Manila at night during 17–22 March 1990.

It is shown that the nighttime weakening of the equatorial zonal electric field, in combination with the corrected equatorward wind-induced plasma drift along magnetic field lines, provides the development of the nighttime enhancements in *Nm*F2 observed over Manila during 17–22 March 1990, bringing the measured and modeled *Nm*F2 into reasonable agreement. As a result, the nighttime weakening of the equatorial zonal electric field and corrected equatorward plasma drift along magnetic field lines, caused by the neutral wind in the both geomagnetic hemispheres, are found to be the new physical mechanisms of the formation of nighttime enhancements in *Nm*F2 close to the geomagnetic equator.

It is shown that the striking increase in *hm*F2 over the Arecibo radar following the F2-peak altitude decrease on 21 March is explained from the model simulations by the large equatorward surge of the meridional neutral wind, which is evaluated to be of 108–127 ms^{-1} from 01:40 UT to 02:30 UT and 158–170 ms^{-1} from 06:30 UT to 08:30 UT on 21 March at 300-km altitude. On the other hand, there are no equatorward wind surges at 300-km altitude over the MU radar derived from the comparison between the measured and modeled F2-peak altitudes close to these time periods on 21 March. We conclude that the results of the model simulations provide evidence in favor of an asymmetry in longitude of the energy input into the auroral region of the Northern Hemisphere.

The calculated *Nm*F2 equatorial anomaly is the longer-lasting phenomenon on 19 March than on 17, 18, 20, 21, and 22 March, and the shortest duration of the equatorial anomaly in *Nm*F2, with both distinguished southern and northern crests occuring on 20 March. The southern crest is more depleted than the northern crest during most of the studied time period. It is shown that the latitudinal positions of the crests depend on the $\boldsymbol{E}\times\boldsymbol{B}$ drift velocity and on the neutral wind velocity. The relative role of the main mechanisms of the equatorial anomaly suppression observed during geomagnetic storms is studied for the first time from the model simulations in terms of storm-time variations of the crest-to-trough ratios. During most of the geomagnetic storm-time period of 18–22 March 1990, a total contribution from meridional neutral winds and the differences between the corrected equatorial zonal electric field used and that produced by the empirical model of Scherliess and Fejer (1999) for quiet conditions to the equatorial anomaly changes is larger than that from geomagnetic storm disturbances in the neutral temperature and densities. The predominant source of the suppression of the equatorial anomaly is related to the wind-induced plasma drift on 19 and 21 March. The changes in the $\boldsymbol{E}\times\boldsymbol{B}$ plasma drift during the time periods of 17, 18, 20 and 22 March (due to the differences between the corrected equatorial zonal electric field used and that produced by the empirical model of Scherliess and Fejer (1999) for quiet conditions) make the largest contribution to the inhibition of the equatorial anomaly. It is shown that geomagnetic storm disturbances in the neutral densities lead to either an enhancement or an inhibition of the equatorial anomaly. Vibrationally excited N_2 and O_2 promote the equatorial anomaly enhancement during the predominant part of the studied time period, however, the relative role of vibrationally excited N_2 and O_2 in the development of the equatorial anomaly is much

less important in comparison with the total effect of the wind-induced plasma drifts and the above-mentioned variations in the $\boldsymbol{E}\times\boldsymbol{B}$ plasma drift. It follows from the model calculations that the asymmetries in the neutral wind and in neutral densities relative to the geomagnetic equator are responsible for the north-south asymmetry in *Nm*F2 and *hm*F2, and for the asymmetry between the values of the crest-to-trough ratios of the Northern and Southern Hemispheres.

The model simulations show that the increase in the loss rate of $O^+(^4S)$ ions, due to vibrationally excited N_2 and O_2, leads to the maximum decrease in the calculated *Nm*F2 by a factor of 1.4 and to the maximum change in the calculated F2-layer peak altitude of 29 km in the low-latitude ionosphere over the ionosonde stations of Table 1 and over the MU radar. The loss rate of $O^+(^4S)$ ions, due to vibrationally excited N_2 and O_2, causes the increase in the calculated electron temperature at *hm*F2 up to the maximum values of 285 K. Over the Arecibo radar, the maximum reduction in the calculated *Nm*F2, due to vibrationally excited N_2 and O_2, is found to be 1.5 and the maximum rise in the calculated electron temperature at *hm*F2 is calculated as 774 K, while the maximum change in the calculated F2-layer peak altitude of 29 km, caused by vibrationally excited N_2 and O_2, is found from the model calculations over Arecibo. Including vibrationally excited N_2 and O_2 in the loss rate of $O^+(^4S)$ ions brings the measured and modeled electron densities and temperatures into reasonable agreement. We found the negligible increase in the calculated ion temperature at *hm*F2, caused by effects of vibrationally excited N_2 and O_2, on the $O^+(^4S)$ ion loss rate (through corresponding changes in N_e and T_e) in the low-latitude ionosphere over the ionosonde stations of Table 1 and over the MU radar during 17–22 March 1990 and over the Arecibo radar for the time period of 20–22 March 1990.

Acknowledgements. The authors of the paper acknowledge B. G. Fejer and L. Schlerliess for providing us by the Fortran codes of the empirical models of the plasma drift over the geomagnetic equator for quiet and disturbed conditions The MU radar belongs to and is operated by RISH. A. V. Pavlov was supported for this work by the Japan Society for the Promotion of Science Invitation Fellowship Program for Research in Japan (Short-Term, ID No. S-05058) and as a Visiting Professor at RISH of Kyoto University. The authors wish to thank the staff of Millstone Hill Observatory of the Massachusetts Institute of Technology for use of the Madrigal Database data. Hourly critical frequencies *fo*f2, *fo*E and maximum usable frequency parameters M(3000)F2 data from the Manila ionospheric sounder station were provided by the National Geophysical Data Center at Boulder, Colorado. Hourly *fo*f2, M(3000)F2, and *fo*E ionospheric parameters measured by the Kokubunji, Yamagawa, and Okinawa sounders were provided from WDC for Ionosphere, Tokyo, National Institute of Information and Communications Technology of Japan, while the Australian Government IPS Radio and Space Service was used to obtain these data by Internet for the Vanimo, and Darwin ionosondes. The authors would like to thank referees for their comments on the paper, which have assisted in improving the final version.

Topical Editor M. Pinnock thanks H. Risbeth and another referee for their help in evaluating this paper.

References

Abdu, M. A., Sobral, J. H. A. de Paula, E. R., and Batista, I. S.: Magnetospheric disturbance effects on the Equatorial Ionization Anomaly (EIA) – an overview, J. Atmos. Terr. Phys., 53, 757–771, 1991.

Abdu, M. A.: Major phenomena of the equatorial ionosphere-thermosphere system under disturbed conditions, J. Atmos. Terr. Phys., 59, 1505–1519, 1997.

Akasofu, S.-I. and Chapman, S.: Solar terrestrial physics, Oxford, Pergamon Press, 1972.

Anderson, D. N.: Modeling the ambient, low-latitude F-region ionosphere – A review, J. Atmos. Terr. Phys., 43, 753–762, 1981.

Anderson, D. N. and Klobuchar, J. A.: Modeling the total electron content observations above Ascension Island, J. Geophys. Res., 88, 8020–8024, 1983.

Aponte, N., González, S. A., Kelley, M. C., Tepley, C. A., Pi, X., and Iijima, B.: Advection of the equatorial anomaly over Arecibo by small-storm related disturbance dynamo electric fields, Geoph. Res. Lett., 27, 2833–2836, 2000.

Bailey, G. J.: The topside ionosphere above Arecibo at equinox during sunspot maximum, Planet. Space Sci., 28, 47–59, 1980.

Balan, N., Bailey, G. J., Nair, B. B., and Titheriedge, J. E.: Nighttime enhancements in ionospheric electron content in the northern and southern ionosphere, J. Atmos. Terr. Phys., 56, 67–69, 1994.

Balan, N., Bailey, G. J., Moffett, R. J., Su, Y. Z., and Titheridge, J. E.: Modelling studies of the conjugate-hemisphere differences in ionospheric ionization at equatorial anomaly latitudes, J. Atmos. Terr. Phys., 57, 279–292, 1995.

Buonsanto, M. J.: Ionospheric storms – a review, Space Science Reviews, 88, 563–601, 1999.

Buonsanto, M. J., Foster, J. C., and Sipler, D. P.: Observations from Millstone Hill during the geomagnetic disturbances of March and April 1990, J. Geophys. Res., 97, 1225–1243, 1992.

Buonsanto, M. J. and Foster, J. C.: Effects of magnetospheric electric fields and neutral winds on low-midddle latitude ionosphere during the March 20–21, 1990 storm, J. Geophys. Res., 98, 19 133–19 140, 1993.

Buonsanto, M. J., González, S. A., Pi, X., Ruohoniemi, J. M., Sulzer, M. P., Swartz, W. E., Thayer, J. P., and Yuan, D. N.: Radar chain study of the May, 1995 storm, J. Atmosph. Sol. Terr. Phys., 61, 233–248, 1999a.

Buonsanto, M. J., González, S. A., Lu, G., Reinisch, B. W., and Thayer, J. P.: Coordinated incoherent scatter radar study of the January 1997 storm, J.Geophys. Res., 104, 24 625–24 638, 1999b.

Burge, J. D., Eccles, D., King, J. W., and Ruster, R.: The effects of thermospheric winds on the ionosphere at low and middle latitudes during magnetic disturbances, J. Atmos. Terr. Phys., 35, 617–623, 1973.

Burnside, R. G. and Tepley, C. A.: Optical observations of thermospheric neutral winds at Arecibo between 1980 and 1987, J. Geophys. Res., 94, 2711–2716, 1989.

Burnside, R. G., Tepley, C. A., and Sulzer, M. P.: World Day observations at Arecibo – 1985 to 1989, J. Geophys. Res., 96, 3691–

3710, 1991.

Chandra, S. and Spencer, N. W.: Thermospheric storms and related ionospheric effects, J. Geophys. Res., 81, 5018–5026, 1976.

Crary, D. J. and Forbes, J. M.: The dynamic ionosphere over Arecibo – A theoretical investigation, J. Geophys. Res., 91, 249–258, 1986.

Dasgupta, A., Anderson, D. N., and Klobuchar, J. A.: Modeling the low-latitude ionospheric total electron content, J. Atmos. Terr. Phys., 47, 917–924, 1985.

Deminov, M. G. and Fishchuk, Ya. A.: On the use of the geomagnetic field approximation by the eccentric dipole in problems of ionosphere and plasmasphere, Geomagnetism and Aeronomy, 40, 383–387, 2000.

Dudeney, J. R.: The accuracy of simple methods for determining the height of the maximum electron concentration of the F2-layer from scaled ionospheric characteristics, J. Atmosph. Terr. Phys., 45, 629–640, 1983.

Emmert, J. T., Fejer, B. G., Fesen, C. G., Shepherd, G. G., and Solheim, B. H.: Climatology of middle- and low-latitude daytime F region disturbance neutral winds measured by Wind Imaging Interferometer (WINDII), J. Geophys. Res., 106, 24 701–24 712, 2001.

Fejer, B. G., Emmert, J. T., and Sipler, D. P.: Climatology and storm-time dependence of nighttime thermospheric neutral winds over Millstone Hill, J. Geophys. Res., 107, pp. SIA 3–1, CiteID 1052, doi:10.1029/2001JA000300, 2002.

Fejer, B. G.: F region plasma drifts over Arecibo – Solar cycle, seasonal, and magnetic activity effects, J. Geophys. Res., 98, 13 645–13 652, 1993.

Fejer, B. G.: Low latitude storm-time ionospheric electrodynamics, J. Atmos. Sol. Terr. Phys., 64, 1401–1408, 2002.

Fejer, B. G. and Scherliess, L.: Empirical models of storm-time equatorial zonal electric fields, J. Geophys. Res., 102, 24 047–24 056, 1997.

Fesen, C. G., Crowley, G., and Roble, R. G.: Ionospheric effects at low-latitudes during the March 22, 1979, geomagnetic storm, J. Geophys. Res., 94, 5405–5417, 1989.

Fraser-Smith, A. C.: Centered and eccentric geomagnetic dipoles and their poles, 1600–1985, Rev. Geophys., 25, 1–16, 1987.

Fox, J. L. and Dalgarno, A.: The vibrational distribution of N_2^+ in the terrestrial ionosphere , J. Geophys. Res., 90, 7557–7567, 1985.

Friedman, J. F. and Herrero, F. A.: Fabry-Perot interferometer measurements of thermospheric neutral wind gradients and reversals at Arecibo, Geophys. Res. Lett., 9, 785–788, 1982.

Fukao, S., Sato, T., Tsuda, T., Yamamoto, M., Yamanaka, M. D., and Kato, S.: MU radar: new capabilities and system calibrations, Radio Sci., 25, 477–485, 1990.

Fuller-Rowell, T. J., Codrescu, M. V., Moffett, R. J., and Quegan, S.: Response of the thermosphere and ionosphere to geomagnetic storms, J. Geophys. Res., 99, 3893–3914, 1994.

Fuller-Rowell, T. J., Millward, G.H., Richmond, A. D., and Codrescu, M. V.: Storm-time changes in the upper atmosphere at low-latitudes, J. Atmos. Sol. Terr. Phys., 64, 1383–1391, 2002.

Gonzalez, W. D. and Tsurutani, B. T.: Criteria of interplanetary parameters causing intense magnetic storms (Dst<–100 nT), Planet. Space Sci., 35, 1101–1109, 1987.

Hocke, K. and Schlegel, K.: A review of atmospheric gravity waves and travelling ionospheric disturbances: 1982–1995, Ann. Geophys., 14, 917–940, 1996.

Hedin, A. E., Spencer, N. W., Biondi, M. A., Burnside, R. G., Hernandez, G., and Johnson, R. M.: Revised global model of thermosphere winds using satellite and ground-based observations, J. Geophys.Res., 96, 7657–7681, 1991.

Hernandez, G. and Roble, R. G.: The geomagnetic quiet nighttime thermospheric wind pattern over Fritz peak observatory during solar cycle minimum and maximum, J. Geophys. Res., 89, 327–337, 1984a.

Hernandez, G. and Roble, R. G.: Nighttime variation of thermospheric winds and temperatures over Fritz Peak Observatory during the geomagnetic storm of March 2, 1983, J. Geophys. Res., 89, 9049–9056, 1984b.

Hierl, M. P., Dotan, I., Seeley, J. V., Van Doren, J. M., Morris, R. A., and Viggiano, A. A.: Rate constants for the reactions of O^+ with N_2 and O_2 as a function of temperature (300–1800 K) , J. Chem. Phys., 106, 3540–3544, 1997.

Jain, S., Vijay, S. K., Gwal, A. K., and Huang, Y. N.: Nighttime enhancements in ionospheric electron content: seasonal and solar cycle variation, Ann. Geophys., 13, 256–261, 1995.

Jenkins, B., Bailey, G. J., Ennis, A. E., and Moffett, R. J.: The effect of vibrationally excited nitrogen on the low-latitude ionosphere, Ann. Geophys., 15, 1422–1428, 1997.

Kawamura, S., Otsuka, Y., Zhang, S.-R., Fukao, S., and Oliver, W. L.: A climatology of MU radar observations of thermospheric winds, J. Geophys. Res., 105, 12 777–12 788, 2000.

Kawamura, S.: A study of wind variations and their effects on the mid latitude ionosphere and thermosphere based on the MU radar observations, PhD Thesis, Radio Science Center for Space and Atmosphere Kyoto University, Japan, 2003.

Krishna Murthy, B. V., Hari, S. S., and Somayajulu, V. V.: Nighttime equatorial thermospheric meridional winds from ionospheric h'F data, J. Geophys. Res., 95, 4307–4310, 1990.

Lanzerotti, L. J., Cogger, L. L., and Mendillo, M.: Latitude dependence of ionosphere total electron content: Observations during sudden commencement storms, J. Geophys. Res., 80, 1287–1306, 1975.

MacPherson, B., González, S. A., Bailey, G. J., Moffett, R. J., and Sulzer, M. P.: The effects of meridional neutral winds on the the O^+-H^+ transition altitude over Arecibo, J. Geophys. Res., 103, 29 183–29 198, 1998.

Nelson, G. I. and Cogger, L. L.: Enhancements in electron content at Arecibo during geomagnetic storms, Planet. Space Sci., 99, 761–775, 1971.

Oliver, W. L., Fukao, S., Sato, T., Tsuda, T., Kato, S., Kimura, I., Ito, I., Saryou, T., and Araki, T.: Ionospheric incoherent scatter measurements with the Middle and Upper Atmosphere Radar: Observations during the large magnetic storm of February 6–8, 1986, J. Geophys. Res., 93, 14 649–14 655, 1988.

Oliver, W. L., Fukao, S., Takami, T., Tsuda, T., and Kato, S.: Four-beam measurements of ionospheric structure with the MU radar during the low-latitude auroral event of 20—23 October 1989, Geophys. Res. Lett., 18, 1975–1978, 1991.

Osterman, G. B., Heelis, R. A., and Bailey, G. J.: Modeling the formation of intermediate layers at Arecibo latitudes, J. Geophys. Res., 99, 11 357–11 366, 1994.

Pavlov, A. V.: The role of vibrationally excited nitrogen in the formation of the mid-latitude negative ionospheric storms, Ann. Geophys., 12, 554–564, 1994.

Pavlov, A. V.: New method in computer simulations of electron and ion densities and temperatures in the plasmasphere and low-latitude ionosphere, Ann. Geophys., 21, 1601–1628, 2003.

Pavlov, A. V. and Buonsanto, M. J.: Comparison of model electron densities and temperatures with Millstone Hill observations during undisturbed periods and the geomagnetic storms of March 16–23 and April 6–12, 1990, Ann. Geophys., 15, 327–344, 1997.

Pavlov, A. V. and Oyama, K.-I.: The role of vibrationally excited nitrogen and oxygen in the ionosphere over Millstone Hill during 16–23 March 1990, Ann. Geophys., 18, 957–966, 2000.

Pavlov, A. V. and Foster, J. C.: Model/data comparison of F region ionospheric perturbation over Millstone Hill during the severe geomagnetic storm of 15–16 July, 2000, J. Geophys. Res., 106, 29 051–29 070, 2001.

Pavlov, A. V., Fukao, S., and Kawamura, S.: Comparison of the measured and modeled electron densities and electron and ion temperatures in the low-latitude ionosphere during 19–21 March 1988, Ann. Geophys., 22, 2747–2763, 2004a.

Pavlov, A. V., Fukao, S., and Kawamura, S.: F region ionospheric perturbations in the low-latitude ionosphere during the geomagnetic storm of 25—27 August 1987, Ann. Geophys., 22, 3479–3501, 2004b.

Pavlov, A. V., and Pavlova, N. M.: Mechanism of the post-midnight winter nighttime enhancements in NmF2 over Millstone Hill during 14–17 January 1986, J. Atmosph. Sol. Terr. Phys., 65, 381–395, 2005a.

Pavlov, A. V. and Pavlova, N. M.: Causes of the mid-latitude NmF2 winter anomaly at solar maximum, J. Atmosph. Sol. Terr. Phys., 67, 862–877, 2005b.

Pi, X., Mendillo, M., Hughes, W. J., Buonsanto, M. J., Sipler, D. P., Kelly, J., Zhou, Q., Lu, G., and Hughes, T. J.: Dynamical effects of geomagnetic storms and substorms in the middle-latitude ionosphere: An observational campaign, J. Geophys. Res., 105, 7403–7418, 2000.

Picone, J. M., Hedin, A. E., Drob, D. P., and Aikin, A. C.: NRLMSISE-00 empirical model of the atmosphere: statistical comparisons and scientific issues, J. Geophys. Res., 107(A12), 1468, doi:10.1029/2002JA009430, 2002.

Pincheira, X. T., Abdu, M. A., Batista, I. S., and Richards, P. G.: An investigation of ionospheric responses, and disturbance thermospheric winds, during magnetic storms over South American sector, J. Geophys. Res., 107(A11), 1379, doi:10.1029/2001JA000263, 2002.

Pinto Jr., O and Gonzalez, W. D.: Energetic electron precipitation at the South Atlantic Magnetic Anomaly – A review, J. Atmosph. Terr. Phys., 51, 351–365, 1989.

Reddy, C. A., Fukao, S., Takami, T., Yamamoto, M., Tsuda, T., Nakamura, T., and Kato, S.: A MU radar-based study of mid-latitude F region response to a geomagnetic disturbance, J. Geophys. Res., 95, 21 077–21 094, 1990.

Richards, P. G., Fennelly, J. A., and Torr, D. G.: EUVAC: A solar EUV flux model for aeronomical calculations, J. Geophys. Res., 99, 8981–8992, 1994. (Correction in J. Geophys. Res., 99, 13 283, 1994a.)

Richards, P. G., Torr, D. G., Buonsanto, M. J., and Sipler, D. P.: Ionospheric effects of the March 1990 magnetic storm: comparison of theory and measurements, J. Geophys. Res., 99, 23 359–23 365, 1994b.

Rishbeth, H.: The effect of winds on the ionospheric F2-peak, J. Atmos. Terr. Phys., 29, 225–238, 1967.

Rishbeth, H.: F region storms and thermospheric circulations, J. Atmos. Terr. Phys., 37, 1055–1064, 1975.

Rishbeth, H.: The equatorial F-layer: progress and puzzles, Ann. Geophys., 18, 730–739, 2000.

Rishbeth, H. and Fukao, S.: A review of MU radar observations of the thermosphere and ionosphere, J. Geomagn. Geoelectr., 47, 621–637, 1995.

Sato, T., Fukao, S., Tsuda, T., Ito, A., and Oliver, W.L.: Ionospheric incoherent scatter measurements with the middle and upper atmosphere radar – Techniques and capability, Radio Science, 24, 85–98, 1989.

Scherliess, L. and Fejer, B. G.: Radar and satellite global equatorial F region vertical drift model, J. Geophys. Res., 104, 6829–6842, 1999.

Schmeltekopf, A. L., Ferguson, E. E., and Fehsenfeld, F. C.: Afterglow studies of the reactions He^+, $He(2^3S)$, and O^+ with vibrationally excited N_2, J. Chem. Phys., 48, 2966–2973, 1968.

Shimazaki, T.: World-wide variations in the height of the maximum electron density of the ionospheric F2 layer, J. Radio Res. Labs. Japan, 2(7), 85–97, 1955.

Souza, J. R., Abdu, M. A., Batista, I. S., and Bailey, G. J.: Determination of vertical plasma drift and meridional wind using the Sheffield University Plasmasphere Ionosphere Model and ionospheric data at equatorial and low-latitudes in Brazil: Summer solar minimum and maximum conditions, J. Geophys. Res., 105, 12 813–12 821, 2000.

Su, Y. Z., Bailey, G. J., and Balan, N.: Night-time enhancements in TEC at equatorial anomaly latitudes, J. Atmos. Terr. Phys., 56, 1619–1628, 1994.

Su, Y. Z., Bailey, G. J., and Balan, N.: Modelling studies of the longitudinal variations in TEC at equatorial-anomaly latitudes, J. Atmos. Terr. Phys., 57, 433–442, 1995.

Su, Y. Z., Bailey, G. J., Oyama, K. I., and Balan, N.: A modelling study of the longitudinal variations in the north-south asymmetries of the ionospheric equatorial anomaly, J. Atmos. Terr. Phys., 59, 1299–1310, 1997.

Takami, T., Oliver, W. L., Richmond, A. D., and Fukao, S.: Ionospheric drift similarities at magnetic conjugate and nonconjugate locations, J. Geophys. Res., 101, 15 773–15 782, 1996.

Tyagi, T. R., Soicher, H., Yeh, K. C., and Tauriainen, A.: The electron content and its variations at Natal, Brazil, J. Geoph. Res., 87, 2525–2532, 1982.

Titheridge, J. E.: Winds in the ionosphere – a review, J. Atmos. Terr. Phys., 57, 1681–1714, 1995.

Unnikrishnan, K., Balachandran N. R., Venugopal, C.: A comparative study of nighttime enhancement of TEC at a low-latitude station on storm and quiet nights including the local time, seasonal and solar activity dependence, Ann. Geophys., 20, 1843–1850, 2002.

Young, D. M. L., Yuen, P. C., and Roelofs, T. H.: Anomalous nighttime increase in total electron content, Planet. Space Sci., 18, 1165–1179, 1970.